Protein and molecular characterization of a clinically compliant amniotic fluid stem cell derived extracellular vesicle fraction capable of accelerating muscle regeneration through the enhancement of angiogenesis

Article

Accepted Version

Stem Cells and Development

Stem Cells and Development: http://mc.manuscriptcentral.com/scd

Protein and molecular characterisation of a clinically compliant amniotic fluid stem cell derived extracellular vesicle fraction capable of accelerating muscle regeneration through the enhancement of angiogenesis

Journal:	*Stem Cells and Development*
Manuscript ID	SCD-2017-0089.R2
Manuscript Type:	Original Research Report
Date Submitted by the Author:	n/a
Keyword:	Amniotic Stem Cells, Satellite Cells, Vasculogenesis
Manuscript Keywords (Search Terms):	secretome, regeneration, muscle, miRNA

Complete List of Authors:
mellows, ben; University of Reading, Biological Sciences
mitchell, robert; University of Reading, Biological Sciences
Antonioli, Manuela; INMI Lazzaro Spallanzani IRCCS
Kretz, Oliver
chamber, david
Zeuner, Marie-Theres
denecke, bernd
musante, luca
ramachandra, durrgah
Debacq-Chainiaux, florence
holthofer, harry
Joch, Barbara
ray, steve
Widera, Darius; Cell biology;
David, Anna; Institute for Women's Health, University College London,
Huber, Tobios
Dengjel, Joern
De Coppi, Paolo; UCL Institute of Child Health, Surgery Unit
patel, ketan

Abstract:
The secretome of human amniotic fluid stem cells (AFSC) has great potential as a therapeutic agent in regenerative medicine. However it must be produced in a clinically compliant manner before it can be used in humans. Here we developed a means of producing a biologically active secretome from AFSCs that is free of all exogenous molecules. We demonstrate that the full secretome is capable of promoting stem cell proliferation, migration and protection of cells against senescence. Furthermore, it has significant anti-inflammatory properties. Most importantly we show that it promotes tissue regeneration in a model of muscle damage. We then demonstrate that the secretome contains extracellular vesicles (EV) that harbour much but not all the biological

	activity of the whole secretome. Proteomic characterisation of the EV and free secretome fraction show the presence of numerous molecules specific to each fraction that could be key regulators of tissue regeneration. Intriguingly we show that the EVs only contain miRNA and not mRNA. This suggests tissue regeneration in the host is mediated by the action of EVs modifying existing, rather than the imposition of new, signalling pathways. The EVs harbour significant anti-inflammatory activity as well as promoting angiogenesis; the latter may be the mechanistic explanation for their ability to promote muscle regeneration after cardiotoxin injury.

Title

Protein and molecular characterisation of a clinically compliant amniotic fluid stem cell derived extracellular vesicle fraction capable of accelerating muscle regeneration through the enhancement of angiogenesis

Authors

Ben Mellows[1] (B.A.D.Mellows@pgr.reading.ac.uk)

Robert Mitchell[1] (tn184969@reading.ac.uk)

Manuela Antonioli[2] (ant.manuela@gmail.com)

Oliver Kretz[3,4,5] (oliver.kretz@uniklinik-freiburg.de)

David Chambers[6] (david.2.chambers@kcl.ac.uk)

Marie-Theres Zeuner[7] (m.zeuner@pgr.reading.ac.uk)

Bernd Denecke[8], (bernd.denecke@rwth-aachen.de)

Luca Musante[9] (luca.musante@hotmail.com)

Durrgah Ramachandra[10] (durrgah.ramachandra.09@ucl.ac.uk)

Florence Debacq-Chainiaux[11] (florence.chainiaux@unamur.be)

Harry Holthofer[9,12] 9 (harry.holthofer@helsinki.fi)

Barbara Joch[5] (Barbara.joch@anat.uni-freiburg.de)

Steve Ray[13] (ray.steve1@googlemail.com)

Darius Widera[7] (d.widera@reading.ac.uk)

Anna L David[14,15] (a.david@ucl.ac.uk)

Tobias B. Huber[3,4,12,,16] (thuber@uke.de)

Joern Dengjel[12,17] (joern.dengjel@unifr.ch)

Paolo De Coppi[10, 18] (p.decoppi@ucl.ac.uk)

Ketan Patel[1, 12] (ketan.patel@reading.ac.uk)

Affiliation and addresses

1 School of Biological Sciences, University of Reading, Reading, UK

2 I.N.M.I. L Spallanzani IRCCS, Rome, Italy

3 Department of Medicine III, Faculty of Medicine University Medical Center Hamburg-Eppendorf, Hamburg, Germany

4 Renal Division, Medical Centre, Faculty of Medicine, University of Freiburg, Freiburg, Germany

5 Department of Medicine IV, Faculty of Medicine, University of Freiburg, Freiburg, Germany

6 Wolfson Centre for Age Related Diseases, King's College, London, UK

Mary Ann Liebert Inc., 140 Huguenot Street, New Rochelle, NY 10801

7 School of Pharmacy, University of Reading, Reading, UK

8 Interdisciplinary Centre for Clinical Research Aachen, RWTH Aachen University, Aachen, Germany

9 Centre for Bioanalytical Sciences (CBAS), Dublin City University, Dublin, Ireland

10 Stem Cells & Regenerative Medicine Section, UCL Great Ormond Street Institute of Child Health, London, UK

11 URBC, Namur Research Institute for Life Science (NARILIS), University of Namur, Namur, Belgium.

12 FRIAS Freiburg Institute for Advanced Studies, University of Freiburg, Freiburg, Germany

13 Micregen, Biohub, Alderley Park, Alderley Edge, Cheshire, UK

14 Institute for Women's Health, University College London, London, UK

15 NIHR University College London Hospitals Biomedical Research Centre, London

16 BIOSS Centre for Biological Signalling Studies and Centre for Systems Biology (ZBSA), Albert-Ludwigs-University, Freiburg, Germany

17 Department of Biology, University of Fribourg, Fribourg, Switzerland

Running title

Amniotic fluid stem cell secretome promotes muscle regeneration

Corresponding Author details:

Professor Ketan Patel

School of Biological Sciences

University of Reading

Reading, UK RG6 6UB

Telephone +44118 378 8079

Email ketan.patel@reading.ac.uk

Footnotes and abbreviations

Amniotic fluid stem cells (AFSC), extracellular vesicles (EV), AFSC conditioned media (AF-CM), amniotic fluid stem cell extracellular vesicles (AF-EV), cluster of differentiation (CD); Human foetal IMR-90 Lung Fibroblast cells (IMR-90), Human Adipose Derived Stem Cells (hADMSCs), Foetal Bovine

Serum (FBS), Tumour necrosis factor alpha (TNF-α), cardiotoxin (CTX), beta galactosidase (β-gal), Tibilalis Anterior (TA), embryonic myosin heavy chain (eMHC), heat shock protein (HSP), RNA-induced silencing complex (RISC)

Abstract

The secretome of human amniotic fluid stem cells (AFSC) has great potential as a therapeutic agent in regenerative medicine. However it must be produced in a clinically compliant manner before it can be used in humans. Here we developed a means of producing a biologically active secretome from AFSCs that is free of all exogenous molecules. We demonstrate that the full secretome is capable of promoting stem cell proliferation, migration and protection of cells against senescence. Furthermore, it has significant anti-inflammatory properties. Most importantly we show that it promotes tissue regeneration in a model of muscle damage. We then demonstrate that the secretome contains extracellular vesicles (EV) that harbour much but not all the biological activity of the whole secretome. Proteomic characterisation of the EV and free secretome fraction show the presence of numerous molecules specific to each fraction that could be key regulators of tissue regeneration. Intriguingly we show that the EVs only contain miRNA and not mRNA. This suggests tissue regeneration in the host is mediated by the action of EVs modifying existing, rather than the imposition of new, signalling pathways. The EVs harbour significant anti-inflammatory activity as well as promoting angiogenesis; the latter may be the mechanistic explanation for their ability to promote muscle regeneration after cardiotoxin injury.

Mary Ann Liebert Inc., 140 Huguenot Street, New Rochelle, NY 10801

Introduction

Stem cells are able to undergo numerous asymmetric cell divisions giving rise to one daughter that reverts to its parental state and the other capable of differentiation [1]. In a classical scenario, the differentiated cell carries out repair of only the resident tissue. However an extensive body of research has shown that in many cases the differentiating cell is multipotent. These findings have been exploited to develop therapies in which one conveniently isolated stem cell population can be used to treat numerous damaged tissues [2,3]. As such, it is assumed that stem cells make a direct cellular contribution to the regenerated tissue. However in many instances following the introduction of stem cells, robust tissue regeneration was evident but with minimal stem cell engraftment [4-6]. This had led to a paradigm shift in our understanding of stem cell mediated tissue repair through the proposition that stem cells secrete molecules which activate host cells that are the cellular mediators of regeneration [7]. The notion of a paracrine effect is supported by many studies which show that stem cells secrete a spectrum of proteins, small RNAs and mRNAs which have biological activity [8-10]. In this scenario, secreted stem cell factors modulate host cellular signalling pathways e.g. promoting an anti-inflammatory response or by protecting against senescence [4,11,12]. A number of studies have shown that factors released by stem cells are packaged in a variety of phospholipid membrane bound extracellular vesicles (EVs), including microvesicles and exosomes [10,13]. Several species of EV, such as exosomes, are shed constitutively but more so during cellular stress [14]. Release of EVs from the cell is believed to enable effective long-range signal transduction by protecting the cargo against degradation. Furthermore it is proposed that molecules on the surface of EVs permit homing to specific tissues, thereby facilitating a degree of target specificity [15].

Numerous studies have focused on identifying an optimal population for stem cell therapies by taking into account differentiation repertoire, ease of isolation, longevity and any associated ethical issues. One particularly attractive source is amniotic fluid derived stem cells (AFSCs). These cells support the regeneration of bone [2], lung [16], kidney [17,18], intestine [4], heart [19] and skeletal muscle [20,21]. They are easily isolated from human amniotic fluid which is routinely collected during clinical prenatal diagnostic procedures such as amniocentesis and which is not associated with any ethical issues. Furthermore human AFSCs have been shown capable of approximately 250 population doublings [22]. However in many reports, regeneration takes place without significant AFSC engraftment again pointing to a paracrine mechanism of action [4,9].

In this study we determined whether a human AFSC secretome collected under conditions concordant with clinical translation would support tissue regeneration. Specifically we wanted to

obviate contamination with non-human proteins/molecules including those found in foetal calf serum. We developed conditions which allowed the collection of a secretome which was not only serum free but induced cellular stress without promoting cell death. Here we report that the human AFSC secretome produced in nutrient free and hypoxic conditions contains a spectrum of proteins and miRNA. The whole secretome protected against senescence and promoted stem cell proliferation and migration. Using reporter cell lines we demonstrate significant anti-inflammatory potential of the human AFSC conditioned media (AF-CM). *In vivo* experiments show that the AF-CM promoted skeletal muscle regeneration. We then isolated and characterised the EV fraction (AF-EV) from AF-CM and showed that it too had anti-inflammatory properties and protects against senescence. We profiled the protein and miRNA cargo of both the EV and non EV fraction and found that each contained specific entities. Importantly we show that AF-EVs were able to promote adult mouse muscle regeneration.

Methods

Ethical Approval Human amniotic fluid samples were collected from women having amniocentesis for prenatal diagnosis for therapeutic purposes in Fetal Medicine Unit of University College London Hospital (UCLH). All patients gave informed written consent to an approved researcher under ethical approval (UCL/UCLH Joint Committee for the Ethics of Human Research, REC Reference: 08/0304). Invasive procedures were performed under ultrasound guidance using sterile equipment. *In vivo* animal experiments were performed under a project license from the United Kingdom (UK) Home Office, in agreement with the Animals (Scientific Procedures) Act 1986.

Animal Maintenance Male wild-type C57BL/6 mice (2-3 month-old) were maintained in accordance with the Animals (Scientific Procedures) Act 1986 (UK). Mice were housed under standard environmental conditions (20–22 °C, 12–12 h light–dark cycle), and were provided with food and water ad libitum.

Cell culture Human amniotic fluid stem cells were harvested from a single amniotic fluid sample based on C-kit expression using MACS (Miltenyi Biotec) following 1 passage. C-kit$^+$ AFSCs were cultured on non-tissue culture treated plastic in α-MEM medium (Gibco, Invitrogen) containing 15% FBS, 1% glutamine and 1% penicillin/streptomycin (Gibco), supplemented with 18% Chang B and 2% Chang C (Irvine Scientific).

U251 cells were cultured in antibiotics- free DMEM (Gibco), 10% FBS, 1% glutamine.

Human foetal IMR-90 Lung Fibroblast cells (IMR-90) were a gift of Dr. Debacq-Chainiaux (University of Namur, Belgium). Cells were used at 27-30 population doublings. IMR-90 cells were cultured in α-MEM medium containing 10% FBS, 1% glutamine and 1% penicillin/streptomycin.

StemPro® Human Adipose Derived Stem Cells (hADMSCs; Life Technologies – lot 2117), derived from a 49 year old female donor were from Stem Pro (lot no. 2117). hADMSCs were cultured in MesenPro RS^{TM} (Gibco), 1% L-glutamine, 1% penicillin/streptomycin.

All cells were cultured at 37 °C with 5% CO_2 and passaged upon reaching 70% confluency unless otherwise stated.

Conditioned media (CM) generation and extracellular vesicle (EV) isolation At 10 passage, AFSCs were pelleted at 300g in 1.5 mL microfuge tubes at a density of 1x10^{6}cells/tube. Cells were incubated in 400µl sterile PBS for 24 hours. Following incubation the cells were pelleted at 300 g for 5 minutes, the supernatant was aspirated, pooled and centrifuged at 2,000 g for 20 minutes. The supernatant (AF-CM) was collected and stored at -20°C. AF-EVs were isolated using sequential

ultracentrifugation of AF-CM at 200,000g using a 70.1Ti fixed-angle rotor (Beckman Coulter) and re-suspending EVs in ultra-centrifuged PBS.

Flow Cytometry Expression of surface markers was assessed using monoclonal antibodies against the cluster of differentiation (CD) antigens: anti-human CD44/Alexa Fluor® 647 (Millipore); anti-human CD73/PE (Biolegend 1:20); anti-human CD90/PE (Millipore 1:20); anti-human CD34/FITC (Millipore 1:10); anti-human CD45/FITC (Biolegend 1:20).

Post-CM generation AFSCs were fixed in 4% paraformaldehyde (Sigma Aldrich) for 20 minutes and non-specific binding blocked with 10% FBS (Gibco) at room temperature. Antibodies were diluted in PBS and incubated with the AFSCs for 1 hour at 4°C. 10,000 events were captured and recorded using the BD Accuri C6 flow cytometer C-sampler. Data was analysed using the FlowJo v10 analysis software (FlowJo LLC).

Adipogenic Differentiation AFSCs were seeded at 4000 cells per cm^2 and grown to 95% confluency. Growth media was then removed, cells were washed once with PBS and cultured for 21 days with Stem XVivo Adipogenic Base Media (R&D Systems) supplemented with Stem XVivo Adipogenic Supplement (100X) according to the suppliers instructions. Cells were stained for 30 minutes with Oil Red O and washed with ddH2O.

Osteogenic Differentiation AFSCs were seeded at 4000 cells per cm^2 and grown to 95% confluency. Growth media was then removed, cells were washed once with PBS and cultured for 21 days with Stem XVivo Osteogenic Base Media (R&D Systems) supplemented with Stem Pro Osteocyte/Chondrocyte basal medium (Life Technologies) according to the supplier's instructions. Calcium staining was carried out for 30 minutes using Alizarin Red S and washed with ddH_2O before capturing images.

Chondrogenic Differentiation For chondrogenic differentiation, $1x10^6$ AFSCs were pelleted at 300g. Cell pellets were cultured in Stem Pro Osteocyte/Chondrocyte basal medium (Life Technologies) supplemented with StemPro Chondrogenesis supplement (Life Technologies) according to the supplier's instructions After 21 days, cells were fixed for 15 minutes in 4% PFA/PBS and washed twice with ddH_2O. Chondrogenic cultures were stained for 1h with Alcian blue at RT. Cell pellets were washed twice for 1 hour in 6:4 ethanol/acetic acid de-stain solution. Pellets were washed once in ddH_2O before freezing and blocking in OCT. 10µm cryo-sections were taken using a Bright OT5000 cryostat. Cells and pellet sections were imaged using a bright field microscope.

SDS-PAGE and Silver Staining Protein concentrations in the CM were determined by using the Bio-Rad protein assay (Bio-Rad). CM protein samples were denatured at 100°C then loaded onto a pre-cast NuPAGE® 4-12% SDS-PAGE (Novex) and run at 100V for 3 hours. Silver Staining was carried out using the SilverXpress® silver staining kit (Invitrogen). Protein bands were imaged using a Syngene G:Box and GeneSys software.

Cellular Proliferation Assay hADMSCs were transferred into 96-well culture plates at a density of 400 cells/well and allowed to adhere for 24 hours. Subsequently, media was removed before replacing with corresponding treatments. Cells were treated for 48 hours then washed with PBS, fixed with 4% PFA/PBS for 15 minutes and then washed again in PBS. Nuclei were stained with DAPI and nuclei counted using a fluorescent microscope (Zeiss A1).

Migration Assay hADMSCs were cultured to reach 100% confluency in 24-well plates. A single scratch was created along the diameter of the well with a p200 tip. Media was then aspirated and cells washed once with PBS before treating with their corresponding media/CM treatments. Plates were immediately positioned onto a time-lapse microscope and images were captured at 3 areas of the wound. Total wound coverage was measured using ImageJ software at T=0 hours and T=9 hours.

Cellular Senescence Assay IMR-90 cells were grown in 12-well plates until 70% confluency. Media was removed and replaced with media containing AF-CM and left for a further 24 hours. Media was removed and cells were stressed for 2 hours with 100µM H_2O_2 in serum free media for 2 hours. Media was removed and cells washed twice with PBS prior to being incubated in 1ml growth media for 48 hours in normal culture conditions. Cells were passaged into 3 wells of a 24-well plate at 800 cells/well. After 24 hours, cells were fixed with 0.2% glutaraldehyde/ 2% PFA for 5 minutes. Subsequently, cells were then washed twice in PBS and incubated with 2.5mg/ml X-Gal solution for 18 hours at 37°C in the dark [23]. Subsequently, wells were rinsed twice with PBS and then twice with methanol before air drying. Cells stained blue were considered senescent and assays visualised using a Zeiss A1 inverted Epi-fluorescent Microscope.

NF-κB p65 Nuclear Translocation Assay U251 cells were cultivated on cell-culture treated cover slips for 24 h. After 24 h pre-treatment with CM, cells were exposed to 10 ng/ml TNF-α for 30 minutes. Cells were washed using PBS and fixed in 4% paraformaldehyde (4% PFA, 15 min, RT). Permeabilisation and blocking was carried out as previously described [24]. NF-κB-p65 was detected

Mary Ann Liebert Inc., 140 Huguenot Street, New Rochelle, NY 10801

by immunostaining with p65 antibody (1:100, sc-8008, Santa Cruz Biotechnology), followed by incubation with Alexa fluor 488 goat anti-mouse IgG secondary antibody (Molecular probes 1:200) and mounting in medium containing 2.5µg/ml DAPI. Imaging was carried out using Zeiss Axioimager Epifluorescence microscope and p65 nuclear pixel intensity was measured using ImageJ software.

NF-κB luciferase gene reporter assays U251 cells (Cell line Service, Eppelheim, Germany) were cultivated in Dulbecco's Modified Eagle Medium (DMEM) high glucose (Sigma-Aldrich) containing 1% L-glutamine (200 mM, Sigma-Aldrich) and 10% FBS (Sigma-Aldrich) at 37◦C. Cells were transduced with the lentiviral pGreenFireTM-NF-κB-GFP-Luciferase Reporter construct (System Biosciences) and functionality was confirmed after puromycin selection (5 µg/ml, Apollo scientific) and clonal growth (data not shown). After cells were treated with 2% CM for 24 h, medium was removed and cells were treated with 10 ng/ml TNF-α. Lysing of the cells was performed after 24 h using cell culture lysis buffer (Promega), and activity of luciferase was measured after applying firefly luciferase reporter assay system (Promega) according to manufacturer's guidelines using Lucy 1 luminometric plate reader (Anthos).

***In Vivo* Cardiotoxin induced Mouse TA Injury and AFSC CM/EV Treatment** C57BL/6 mice (12 week old) were tail vein injected with 100µL either hAFSC CM, hAFSC EV or ultra-centrifuged PBS. 30 Minutes later mice were injected with a total of 30µL 50µM Naja pallida cardiotoxin (CTX) (Latoxan, Valence France) into the *tibialis anterior* (TA). After 5 days mice were sacrificed and TA muscles were collected and immediately frozen.

Histology Frozen Tibialis Anterior (TA) muscles were embedded in Tissue-TEK® OCT compound (PST). 12µM cryo-sections were processed for immunohistochemistry [24]. With the following antibodies were used: monoclonal anti-mouse NF-κB-p65 (Santa Cruz 1:200); monoclonal anti-mouse Pax-7 (Developmental studies hybridoma bank-DSHB 1:1); monoclonal anti-mouse Myosin heavy chain 3 (Santa Cruz biotechnology 1:200); Rat anti-mouse CD31 (Bio-Rad 1:150); Rat anti-mouse F4-80 (Bio-Rad 1:200); polyclonal Rabbit anti-MyoD (Santa Cruz biotechnology 1:200). All primary antibodies were pre-blocked in wash buffer for 30 min prior to use. The following secondary antibodies were used: Alexa fluor 488 goat anti-mouse IgG (Molecular probes 1:200), Alexa fluor 594 goat anti-mouse IgG (Molecular probes 1:200), rabbit anti-Rat HRP (DAKO 1:200).

Uptake of PKH26-stained EVs by IMR-90 cells AF-EV staining was carried out using the PKH26 Red Fluorescent Cell Linker Kit (Sigma). IMR-90 cells cultured until 70% confluency and treated for 3

hours with stained AF-EVs for 3 hours. Cells were washed twice with PBS and EV uptake visualised using a Zeiss Axioimager Epifluorescence microscope.

Sample preparation for Mass Spectrometry (MS) AF-EV and non-EV fraction isolated from AFSCs secretome were obtained as described above. Proteins were suspended in SDS-PAGE loading buffer 1x (NuPAGE, Invitrogen, Darmstadt, Germany), denaturated and reduced with 1 mM DTT for 10 min at 95°C then, alkylated using 5.5 mM iodoacetamide for 30 min at 25°C in the dark. Proteins were resolved by SDS-PAGE using 4-12% Bis-Tris mini gradient gels (NuPAGE, Life Technologies). Each lane was cut into 10 equal slices, proteins therein were in-gel digested with trypsin (Promega). Peptides were extracted, purified by STAGE tips, dried to less than 5µl and re-suspended in 15 µl of 0.5% acetic acid for the MS analysis.

Mass Spectrometry Analysis LTQ Orbitrap XL mass spectrometers (Thermo Fisher Scientific) coupled to an Agilent 1200 nanoflow-HPLC (Agilent Technologies GmbH) were used to measure peptides derived from trypsin digestion. Samples, applied directly onto self-packed HPLC-column tips of around 20 cm, were subjected to a gradient formed by solution A (0.5% acetic acid in LC-MS grade water) and by increasing organic proportion of solution B (0.5% acetic acid in 80% LC–MS grade ACN in water) within 120 min [25]. MaxQuant software version 1.4.1.2 was used to identify proteins based on peptides and to perform label-free quantification [26]. Both mass spectrometry and MaxQuant parameters were set as previously described [27]. The analysis of Molecular Function GO terms was performed trough Perseus software version 1.5.8.5 using Fisher's exact test with a p-value threshold of 0.02 [28].

miRNA Array and analysis GeneChip® miRNA 4.0 Arrays were used to analyze the miRNA content of AF-EVs using FlashTag™ Biotin HSR RNA Labeling Kits according to the manufacturer´s instructions. Probe cell intensity data (CEL) from Affymetrix GeneChip® miRNA 4.0 Arrays were analyzed in the Affymetrix Expression Console™ software. Normalization was performed using the Robust Multichip Analysis (RMA) + DABG algorithm [29]. Only miRNAs calculated as present in all 3 samples were declared as generally expressed after 24 hours. Focus was given to the miRNAs present with the highest signal intensities (top 50). For these top 50 miRNAs validated target mRNAs were amalgamated using miRWalk2.0 software [30]. In the next step, GO Slim classification for biological process was performed using WebGestalt software to provide a high-level functional classification for validated target mRNAs [31]. Morpheus software was used to design the Heat-map showing intensity variability between biological replica (n=3) for the top 50.

Transmission Electron Microscopy For TEM extracellular vesicle pellets were re-suspended in 40 µl of 0.1M PBS. Drops of these suspensions were placed on parafilm. Carbon-coated copper meshed grids (Plano, Germany) were placed on the drops for 5 minutes for probe adsorption. After five minutes of fixation on drops of 1% glutaraldehyde (Roth, Germany) grids were washed 4 times for 30 seconds and negative contrasted using 1% uranyl acetate. Grids were air dried and analysed using a Zeiss 906 transmission microscope (Zeiss, Germany).

Statistics All experiments were performed three times unless otherwise stated. Statistical analysis was performed using GraphPad Prism software. Data analysed between multiple groups was tested using one-way ANOVA followed by Tukey's post-hoc testing. For comparison between two groups, independent sample t-tests were completed. Significance values were always set at the 95% confidence interval. All p values were indicated as $p < 0.05$ (*), $p < 0.01$ (**) or $p < 0.001$ (***). All data are displayed as mean ± SEM.

Results

AFSCs retained multipotency following the collection of AF-CM rich in protein and nucleic acid (Figure 1)

AF-CM contained a high level of protein (834.25µg/ml ± 72.73) and a low level of nucleic acid (21.93µg/ml ± 2). Human AFSCs retained expression (Figure 1A-C) of mesenchymal stem cell markers CD44 (97.5%), C73 (92.7%), CD90 (42.7%) whilst being negative (Figure 1D-E) for CD45 (0.095%) and CD34 (5.92%). Following the collection of AF-CM under non physiological conditions, human AFSCs not only survived but were still able to expand in normal culture conditions. Additionally, human AFSCs cultured under differentiating conditions after CM collections were capable of undergoing adipogenesis, osteogenesis and chondrogenesis (Figure 1F-H') confirming their multipotent differentiation capabilities.

AF-CM is able to suppress NF-κB signalling (Figure 2A-E)

The ability of AF-CM to modulate the inflammatory response was tested using U251 cells stimulated with TNF-α which resulted in an increase of nuclear NF-κB p65 (Figure 2D). Treatment with AF-CM for 24 hours before and during TNF-α stimulation led to a reduction in nuclear p65 by 42.5% from 2.28±0.02 to 1.31±0.11 (Figure 2D), at levels comparable to unstressed U251 control cells. Activity of NF-κB activity was quantitatively demonstrated using a NF-κB – Luciferase/GFP lentiviral infected

Mary Ann Liebert Inc., 140 Huguenot Street, New Rochelle, NY 10801

U251 cells (Figure 2E). TNF-α elevated the levels of NF-κB dependent luciferase by 46.3%, which was reduced by 15.4% to 40±1.63 with AF-CM. AF-CM treatment alone showed no change in NF-κB dependent luciferase activity compared to non-TNF-α stimulated control U251 cells. Therefore AF-CM attenuates NF-κB activity, a transcription factor widely regarded to regulate pro-inflammatory signalling [32].

AF-CM modulates exogenous stem cell properties and protect against cellular stress (Figure 2F-G)

The efficacy of AF-CM as a regulator of cellular behaviour was assessed by examining three properties: (i) the ability to reduce levels of cellular senescence, (ii) promote proliferation and (iii) migration. Firstly, we demonstrated a reduction in H_2O_2-induced senescence associated β-gal staining (Figure 2F) following AF-CM treatment stress exposure, from 88.75%±4.39 to 73.25%±1.89. Additionally, AF-CM increased the proliferation capability of Adipose Derived Mesenchymal Stem Cells (ADMSCs) at a range of concentrations (Figure 2G). The 30% increase in cell number attributed to the lowest concentration of AF-CM was similar to changes seen with higher CM concentrations, but 2.5% AF-CM induced the optimal increase in ADMSC migration in a wound closure assay (Figure 2H). Therefore AF-CM demonstrates an ability to protect against senescence induced through stress as well as to promote the proliferation and migration of allogeneic stem cells.

AF-CM enhances regeneration in an *in-vivo* acute muscle injury model (Figure 3)

In order to directly assess its regenerative capabilities, AF-CM was intravenously injected into mice prior to injecting *naja mossambica mossambica* CTX intra-muscularly into the *Tibilalis Anterior* (TA). Expression of eMHC was used to identify newly regenerating muscle fibres (Figure 3A). Analysis of regenerating fibre cross sectional area (CSA) showed a dramatic 73.6% increase in fibre size (from 381.12±4.43μm^2 to 661.67±6.31 μm^2) in the AF-CM treated mice (Figure 3B-C) particularly in those fibres sized 600μm. Since CTX does not directly affect the resident satellite cell population, endogenous stem cells become activated following fibre damage, subsequently differentiated into myoblasts and then fused to replace lost muscle fibres. Although the levels of quiescent Pax7$^+$/MyoD$^-$ and activated Pax7$^+$/MyoD$^+$ satellite cells did not significantly differ between CTX and CTX AF-CM treated mice, the level of muscle lineage committed Pax7$^-$/MyoD$^+$ progenitor cells was increased 76.4% in AF-CM treated mice (28.45±4.66 cells to 50.20±5.62 cells) compared to CTX treated controls (Figure 3D-E). Additionally, AF-CM treated mice had increased numbers of CD31 positive capillaries per area of regenerating muscle (Figure 3G). More importantly the number of CD31$^+$ positive vessels per fibre was increased 75% (from 0.96±0.10 to 1.68±0.25) when compared to the CTX treated controls (Figure 3H). Further examination uncovered a larger infiltration of cells

Mary Ann Liebert Inc., 140 Huguenot Street, New Rochelle, NY 10801

expressing the pan macrophage marker, F4-80^{+}, within TA muscles of AF-CM treated mice compared to control CTX damaged mouse TAs (Figure 3I-J).

AF-CM extracellular vesicle size is characteristic of exosomes and they are rich in miRNA (Figure 4)

Step-wise ultracentrifugation was used to isolate the extracellular vesicles (AF-EV) from the AF-CM. The RNA profile showed that the AF-EV fraction was almost exclusively made up of small species (~21-25 nucleotides in size (Figure 4A)). Small RNAs such as miRNA are known to be vulnerable to enzymatic breakdown and have been proposed as being contained within extracellular vesicles released by cells for inter-cell communication [33,34]. Size analysis of vesicles was originally carried out to determine the type of vesicle being secreted by the AFSCs AF-CM (Figure 4B-C). Average vesicle diameter was 72.5±4.66 nm suggesting that the majority were exosomes. Levels of protein within the AF-EV were found to be very high (595 µg/ml). Vesicular proteins in the AF-EV were compared to those found in the whole AF-CM using silver staining (Figure 4D). Silver staining of proteins in the AF-EV revealed a higher concentration of proteins within the 40-50kDa range compared to the wide spectrum of proteins found in the AF-CM (Figure 4D). Fluorescent red PKH26 stained AF-EVs were taken up by IMR-90 target cells and staining was found situated within the cells as opposed to the cell membrane (Figure 4E).

AF-CM extracellular vesicles protect against cellular stress and suppress NF-κB activation (Figure 5)

In vitro assays testing cellular protection from senescence and ability to reduce NF-κB activity were carried out to compare the AF-EV fraction to the whole AF-CM. The p65 nuclear translocation assay (Figure 5A-E) showed the AF-EV provided a 34.3% greater suppressive effect on the translocation compared to AF-CM (1.47±16.15 and 2.39±0.12 respectively). Quantitative evaluation of AF-EV NF-κB activity via the luciferase based assay showed no change in luciferase expression compared to the AF-CM, (Figure 5F). The AF-EV fraction induced a decrease in the levels of H_2O_2-induced senescence by 78% (from 35.50±1.99 to 7.58±0.94, Figure 5G). However, there were no differences in senescence between the whole and AF-EV fractions.

AF-EV retain the ability to enhance regeneration within an acute muscle injury model *in-vivo* (Figure 6)

Regeneration of CTX damaged TA muscle was used to determine whether the AF-EV fraction promoted muscle regeneration. CSA of newly regenerating TA fibres was increased by AF-EV treatment compared to the CTX damage control (926.66µm^2±24.23 and 484.51µm^2±68.27 respectively), resulting in a 91.2% increase in size of newly formed fibres (Figure 6A-B). Levels of

CD31$^+$ capillaries/fibre (Figure 6C-D) were also increased 29.7% (from 1.01±0.08 to 1.31±0.07 capillaries/fibre) by the AF-EV treatment compared to the vehicle treatment. AF-EV treatment likewise amplified capillary density towards that similarly seen in an undamaged control mirroring what was observed AF-CM. On the other hand, levels of F4-80$^+$ cells were not altered by the AF-EV treatment (Figure 6E-F). AF-EV treatment did not alter the levels of quiescent (Figure 6G), activated satellite cells (Figure 6H) and committed progenitor cells (Figure 6I) compared to that of the CTX damage control. *In vivo* analysis of AF-EV regenerative capabilities showed that treated mice presented with increased vascularisation and regenerating fibres with a larger CSA following CTX damage compared to vehicle treated controls.

AF-EV harbour unique proteins and regeneration promoting miRNA (Figure 7-8)

Mass spectrometry was used to identify proteins in both the AF-EV and non-EV fraction from the human AFSCs secretome (Figure 7B). A total of 856 protein groups were identified. A variety of proteins were found present in both the soluble fraction and EV fraction of the AF-CM (Figure 7A). However, a very distinctive quantitative protein profile was found in the EV fraction compared to the soluble fraction (Figure 7B). 416 protein species were shared between the two fractions. However 250 protein species were unique to the soluble fraction whereas 190 species were exclusive to the AF-EV fraction (Figure 7a). Proteins enriched in the different AF-CM fractions were shown to be important in shared cellular processes (Table 1), cellular processes individual to that of the soluble fraction (Table 2) and processes only found to be controlled by proteins within the AF-EV fraction (Table 3). Of interest were the Heat-Shock family of proteins present in the AF-CM. A large number of Heat-Shock proteins were secreted, some of which were found only within the AF-EV fraction including HSPA (70kDa)-4L, whereas others were found only in the soluble fraction including the mitochondrial 60 kDa heat shock protein (HSPD-1). Finally many were found in both fractions e.g. HSPA-6 protein. Transmembrane transporters and receptors were enriched within the AF-EV including ABCE1, ABCF1, ABR, AP2A1, CYFIP1, CYFIP2, DNM1, DNM2, DNM3, HDAC2, HDAC1, HK1, MAPK1, NCKAP1, PPP1CB, ROCK2, RTN4, STRAP, USP9X, USP9Y and XPO1 (7B). A2B1 ribonucleoprotein was also found in the AF-EV fraction, whilst no RISC complex associated proteins were found in either fraction.

Detailed analysis of the AF-EV miRNA led to the identification of 586 miRNA species and 21399 pathway targets (Figure 8B). The majority of miRNA were found to target mRNA controlling processes such as metabolic activity (Figure 8B) but also more specifically responses to stress (Figure 8C). Within the top 50 miRNAs in the AF-EV, many were postulated to promote angiogenesis,

proliferation, migration, differentiation and autophagy such as miR382, miR24-3p and miR3960 [35-37]. Other species of miRNA found potentially inhibit apoptosis, including miR3196, miR762, miR125b-5p and miR1273-3p [38-41]. Whilst others present such as miRNA let-7b-5p are known to also possess anti-inflammatory effects [42,43].

Discussion

Our extensive characterisation of AF-CM and its AF-EV fraction created under non-physiological conditions from human AFSCs provides crucial information about their protein and RNA cargo. We demonstrated that human AFSC derived AF-CM and AF-EV were able to modulate allogeneic stem cell activity and inflammatory signalling. Our results showed that alterations in inflammatory signalling following treatment with AF-CM were mediated at least in part through NF-κB pathway repression. Furthermore, our data suggests that many paracrine factors that support regeneration were in the AF-EV. Interestingly, the RNA fraction of the secretome was made entirely of miRNA and lacked mRNA molecules.

Much promise surrounds the clinical potential for MSCs in regenerative therapies. Foetal derived MSCs, such as AFSCs may have greater differentiation potential compared to their adult counterpart, such as adipose derived MSCs [22]. AFSCs are multipotent and promote regeneration of an array of tissues [4,9,22]. However, the ability of AFSCs and other stem cells to regenerate tissue is often through the paracrine acting secretome which include proteins and RNA molecules [4,8]. Paracrine factors are often found in membrane bound vesicles such as exosomes and microvesicles that aid transit for cell communication and protect the cargo from degradation [34]. Low levels of basal EV secretion are often increased after stress [14]. The ability to increase EV shedding following stress was proposed as a means to produce a more potent secretome [44]. Additionally, cell-free based therapies reduce the risk of immunological reactivity often associated with the use of whole cells. The potential for tumorigenesis using whole cells is also avoided and it is believed that cell-free therapies are a safer option for clinical use.

Previous studies have either used whole stem cells or basal medium and/or serum derived CM collected under physiological conditions [4,10]. Collection of AF-CM in PBS, at room temperature as used in this study was postulated to induce cellular stress which would enhance the secretion of regenerative molecules [44]. It concords with a recent study which demonstrated that hypoxia promoted EV secretion from human AFSCs [45]. However in our study, we used even more severe conditions and demonstrated that not only did the human AFSCs survive 24 hours in non-optimal

Mary Ann Liebert Inc., 140 Huguenot Street, New Rochelle, NY 10801

nutrients, temperature and oxygen conditions but they still expressed multipotency markers CD90, CD73 and CD44 as well as retaining the adipogenic, osteogenic and chondrogenic potential. These results show that human AFSCs are extremely resilient which would be beneficial for not only surviving in a hostile cellular environment, which might exist in the uterus during gestation, but also in damaged tissue.

A wealth of evidence shows that paracrine factors released by stem cells are packaged into small membrane bound EVs [10,34,46-48]. We isolated vesicles from our AF-CM which exhibited an average diameter of 72.5nM which is consistent with them being exosomes rather than microvesicles [34,49]. Protein analysis also provided evidence for the presence of exosomes due to the existence of known structure specific markers such as CD63, HSP70, HSP90, ACTB, GAPDH and 14-3-3 protein zeta/delta (YWHAZ) [50,51]. AF-EV cargo profiling identified a number of polypeptides unique to this fraction. Presence of specific proteins within the AF-EV fraction and soluble fraction implies that both may have therapeutic value and contrasts suggestions promoting the use of AF-EV fractions alone [45]. Our data shows that although the AF-EV may provide the AF-CMs principle effects, the use of the AF-EV alone could lead to the loss of potentially important protein species for regeneration.

The library of excreted paracrine factors identified using mass spectrometry suggests that they alter the cellular signalling activity in target cells. Identification of Heat-shock proteins was of particular interest. For example the presence of Heat-shock protein 70 in the AF-CM which has been previously shown to initiate a preparatory like signalling mechanism in order to brace cells for incoming stress [52-54]. Furthermore, the 'alarmin' protein HMGB1 was present in the CM which may further potentiate the protective mechanisms [55]. A reduction in the level of H_2O_2-induced senescence following AF-CM treatment also showed a protective effect. The suggestion that there is a safe guarding against cellular stress following tissue necrosis could in part be explained by the presence of these alarmins within the AF-CM. *In-vitro* experiments showed that AF-CM increased proliferation and migration of ADMSCs, thus showing an ability to modulate allogeneic stem cell activity in favour of regeneration. AF-CM caused no aggravation of a pro-inflammatory response in itself. Interestingly, a capacity to reduce NF-κB-p65 nuclear translocation and TNF-α driven NF-κB activity, demonstrated the ability of AF-CM to reduce inflammation, a key characteristic required for regeneration [56].

Our work also sheds light into the possible role of AFSCs in their natural environment, the amniotic fluid. It has been shown that there is an increase in p65 signalling towards the end of a pregnancy which is believed to help trigger labour. It is conceivable that AFSCs play a role in dampening p65

signalling and therefore prevent pre-term labour but also constrain a pro-inflammatory environment known to be damaging for the foetus [57-59]. We suggest that this is a regulated process such that periods of stress promote the secretion of anti-inflammatory molecules by AFCs into the amniotic fluid.

Treating IMR-90 cells with PKH26 stained AF-EVs not only showed that AF-EVs were capable of being taken up by target cells but it also provided further evidence that uptake was via an active process. The lack of stained membrane lipid around the periphery of the cell and instead presence within the cell suggests that the AF-EV membranes did not fuse with the target cell membrane. Instead its uptake has been proposed to be facilitated by active mechanisms such as endocytosis, preparing cargo endocytic compartment sorting [60,61]. Membrane bound receptors and transporters are thought to aid the facilitation of EV fusion and uptake into target cells [34]. It has been previously hypothesised that EV adsorption is cell specific enabling cellular responses such as angiogenesis [34,48]. Endothelial progenitor derived EVs targeting to endothelial cells is believed to be facilitated by surface alpha4 and beta1 integrins [48]. In contrast, our data shows a regenerative response for the AF-CM and AF-EV in a number of cell types. In keeping with this, mass spectrometry profiling failed to find any specific cell surface targeting protein. These data therefore provide evidence that the AF-CM protective effects are not specific to one cell type but afford cellular protection to a spectrum of cell types. Again this is hypothesised to be of benefit during pregnancy to protect the foetus. This suggests that AF-CM may be therapeutically amenable for use in a number of pathological situations and tissues.

The A2B1 ribonucleoprotein is known to transport miRNA into EVs. The presence of this protein in the AF-EV fraction supports the idea that loading of the miRNA in this compartment is a regulated process [62]. miRNA must be protected for long range transport and signalling due to their instability and susceptibility to enzymatic degradation. Protection can be facilitated via interaction with the RISC protein complex. However, mass spectrometry failed to detect RISC complex proteins. We suggest the role of providing miRNA stability is fulfilled by EVs. Packing of miRNA into EVs not only protects them from degradation but may be essential for their biological action. Indeed recent research has demonstrated that naked circulating miRNA has no biological activity. This property is imbued following their encasement in EV [13]. One very important finding of this study was that all the RNA in the CM was miRNA with no evidence of mRNA [33,48,63,64]. This signifies that AF-CM modifies endogenous programmes of the existing target cells rather than imposing ones that are completely foreign.

Mary Ann Liebert Inc., 140 Huguenot Street, New Rochelle, NY 10801

Enhanced regenerative properties of the EV fraction demonstrated here could be attributed to the presence of miR125b-5p, miR3196 and miR762, which target pro-apoptotic and senescence related mRNA [40]. Suppression of keap1 mRNA by miRNA125b-5p has been shown to inhibit both FAS induced apoptosis and APAP induced necrosis leading to the inhibition of acute liver failure [40]. In addition, targeting of the RNF4 gene by miR762 inhibits apoptosis by inducing DNA repair mechanisms [39]. The modulation of H2AX expression by miR3196 and downregulation of PUMA/p53/p21 signalling was shown to inhibit apoptosis but also suggests a subsequent suppression of downstream senescence [38]. Importantly some of the identified miRNAs, notably Let-7b, have been previously shown to be anti-inflammatory [42]. A recent study by Balbi et al profiled miRNA in a AF-CM with regenerative properties [45]. However none of their candidates feature on the list of top 50 miRNA found in our samples. We suggest that the types of miRNA produced by human AFSCs depend on culture conditions and many miRNA regulate mRNA that control regeneration.

Suppression of NF-κB signalling by the AF-EV fraction was shown to be equal to, or stronger than that of the whole AF-CM. This implies that the components subduing NF-κB activity reside mainly in the EV fraction. Our data provides direct evidence of AF-CM and AF-EV having anti-inflammatory effects through suppression of NF-κB signalling. Studies into the ability of AFSC CM to alter the polarisation of M1 to M2 macrophages will provide further evidence of its anti-inflammatory ability as was shown recently with adipose derived MSC CM [65]. Cellular protection may also derive from the vesicular portion of the CM as evidenced by a reduction in cellular senescence with AF-EV being equally potent as AF-CM. The regulation of NF-κB signalling homesis is important in both the determination of the inflammatory response but also many other directly and indirectly related pathways such as cellular growth, proliferation and the stress response [66,67]. These results suggest that the AF-CM including its EV fraction may drive signalling towards a normal equilibrium like-state.

Our results show that both the CM and EV from AF cells promote muscle regeneration. However we believe that the subtle differences in the results from these two experiments offer not only mechanistic insights into how this is occurring but also the relative importance of differing factors in the process. Whole CM experiment showed an increase in the number of committed muscle cells ($Pax7^{+}/MyoD^{+}$), an increase in capillary density and increased number of macrophages. Capillary density but not macrophage infiltration was changed in the EV experiment compared to controls. Furthermore in the EV experiment, the number of activated precursor muscle cells was increased. These results suggest that the supra-basal infiltration of macrophages is not a key determinant in

this study to the enhanced fibre regeneration effect of AF-CM or AF-EV. AF-CM and AF-EV treatments both increased the capillary density. A highly vascularised tissue is documented to support regeneration [68]. Indeed recent work shows that an enhancement in vascularisation can overcome even a deficit in muscle stem cell numbers to promote muscle regeneration [68]. We suggest that the impressive enhancement in muscle regeneration seen after AF-EV treatment is due to a combined effect of not only increased capillary density but also an increase in the number of $Pax7^{+}/MyoD^{+}$ cells. A number of studies have shown that these cells undergo more rapid division than committed $Pax7^{-}/MyoD^{+}$ cells [69]. We suggest that constant supply of precursors in a highly vascularised environment, promoted by AF-EV, results in superior regeneration compared to AF-CM treatment.

Notably, our *in vitro* results were in general accordance with the data obtained in the *in-vivo* model of muscle regeneration. Our data showed that both AF-CM and AF-EVs accelerated muscle regeneration after CTX damage. The most obvious sign of regeneration was the enhanced CSA of newly regenerating fibres 5 days after damage. Both the AF-CM and AF-EV doubled the size of regenerating fibres. Our data directly showed significant evidence of increased levels of capillary density following AF-CM (3F-H) and AF-EV (8C-D) [45]. The level of angiogenesis during regeneration has been suggested as being more important than the number of satellite cells present [68]. Let7b has been linked to function as a pro-angiogenic miRNA as well as miR382, which was also found to be present and previously demonstrated to promote angiogenesis via PTEN repression [35,43]. The increase in $F4\text{-}80^{+}$ cells following AF-CM treatment could be due to the time frame in which muscles were collected following damage. Hypothetically the increase in macrophage numbers is due to a surge in anti-inflammatory M2 macrophages. However, unlike the AF-EV, the AF-CM significantly elevated the number of $Pax7^{-}/MyoD^{+}$ myogenic committed progenitor cells. A greater level of committed cells in the CM treated mice along with the increased exogenous stem cell migration and proliferation *in-vitro* evokes the possibility that AF-CM enhances satellite cell proliferation and migration. This would lead to increased levels of myogenic committed cells seen 5 days later upon dissection. More myogenic progenitor cells would also account for an increased fibre size due to elevated myoblast fusion events. To summarise, the whole AF-CM had an ability to increase regenerating fibre size, increased the number of capillaries/fibre and increase the level committed muscle progenitors available. On the other hand, the AF-EV was shown only to retain the ability to increase the regenerating fibre size and the number of capillaries/fibre. Although AF-EV fraction is able to promote regeneration, these results imply that the use of whole AF-CM may be more beneficial therapeutically than AF-EV fraction alone because it mediated wider regenerative

Mary Ann Liebert Inc., 140 Huguenot Street, New Rochelle, NY 10801

effects. The array of factors both in the soluble and AF-EV fraction could provide more means of regeneration compared to that of the AF-EV alone. On the other hand, in the case of miRNA, there is strong evidence suggesting that it can only significantly alter the signalling of other cells when packaged, secreted and intercepted within EVs [13].

In summary we show that AF-CM produced from human AFSCs under conditions compliant with clinical translation contained a spectrum of proteins and miRNA as the predominant molecular species. The secretome was shown to regulate key stem cell activities as well as promoting skeletal muscle regeneration. AF-CM contained exosomes which carried a unique cargo which in itself was able to promote muscle regeneration. Proteomic and molecular profiling of the cargo identified molecules capable of modulating inflammation and angiogenesis which could mechanistically underpin tissue regeneration. Future investigations will focus on specific cargo molecules for their ability to promote the repair of tissue.

Acknowledgments

This research was funded by BBSRC, National Institutes for Health Research Great Ormond Street Biomedical Research Centre and Rosetrees Trust.

ALD is funded by the National Institute for Health Research University College London Hospitals Biomedical Research Centre. PDC is funded National Institute for Health Research and Great Ormond Street Hospital Children's Charity.

TBH was supported by the DFG (CRC1140, CRC 992, HU 1016/8-1), by the BMBF (01GM1518C), by the European Research Council-ERC grant 616891 and by the H2020-IMI2 consortium BEAt-DKD. DW was supported by a grant of the DFG (WI4318/2-1).

Author Disclosure Statement

No competing financial interests exist for any of the authors involved in this study.

References

1. Weissman IL. (2000). Stem Cells: Units of Development, Units of Regeneration, and Units in Evolution. Cell 100:157-168.
2. Ranzoni AM, M Corcelli, KL Hau, JG Kerns, M Vanleene, S Shefelbine, GN Jones, D Moschidou, B Dala-Ali, AE Goodship, P De Coppi, TR Arnett and PV Guillot. (2016). Counteracting bone fragility with human amniotic mesenchymal stem cells. Sci Rep 6:39656.
3. Okamoto R, T Yajima, M Yamazaki, T Kanai, M Mukai, S Okamoto, Y Ikeda, T Hibi, J Inazawa and M Watanabe. (2002). Damaged epithelia regenerated by bone marrow-derived cells in the human gastrointestinal tract. Nat Med 8:1011-7.
4. Zani A, M Cananzi, F Fascetti-Leon, G Lauriti, VV Smith, S Bollini, M Ghionzoli, A D'Arrigo, M Pozzobon, M Piccoli, A Hicks, J Wells, B Siow, NJ Sebire, C Bishop, A Leon, A Atala, MF

Lythgoe, A Pierro, S Eaton and P De Coppi. (2014). Amniotic fluid stem cells improve survival and enhance repair of damaged intestine in necrotising enterocolitis via a COX-2 dependent mechanism. Gut 63:300-9.

5. Yang DY, ML Sheu, HL Su, FC Cheng, YJ Chen, CJ Chen, WT Chiu, JJ Yiin, J Sheehan and HC Pan. (2012). Dual regeneration of muscle and nerve by intravenous administration of human amniotic fluid-derived mesenchymal stem cells regulated by stromal cell-derived factor-1alpha in a sciatic nerve injury model. J Neurosurg 116:1357-67.
6. Shabbir A, D Zisa, G Suzuki and T Lee. (2009). Heart failure therapy mediated by the trophic activities of bone marrow mesenchymal stem cells: a noninvasive therapeutic regimen. Am J Physiol Heart Circ Physiol 296:H1888-97.
7. Gnecchi M, H He, OD Liang, LG Melo, F Morello, H Mu, N Noiseux, L Zhang, RE Pratt, JS Ingwall and VJ Dzau. (2005). Paracrine action accounts for marked protection of ischemic heart by Akt-modified mesenchymal stem cells. Nat Med 11:367-8.
8. Gnecchi M, P Danieli, G Malpasso and MC Ciuffreda. (2016). Paracrine Mechanisms of Mesenchymal Stem Cells in Tissue Repair. Methods Mol Biol 1416:123-46.
9. Loukogeorgakis SP and P De Coppi. (2016). Stem cells from amniotic fluid – Potential for regenerative medicine. Best Practice & Research Clinical Obstetrics & Gynaecology 31:45-57.
10. Mead B and S Tomarev. (2017). Bone Marrow-Derived Mesenchymal Stem Cells-Derived Exosomes Promote Survival of Retinal Ganglion Cells Through miRNA-Dependent Mechanisms. STEM CELLS Translational Medicine:n/a-n/a.
11. Waterman RS, SL Tomchuck, SL Henkle and AM Betancourt. (2010). A New Mesenchymal Stem Cell (MSC) Paradigm: Polarization into a Pro-Inflammatory MSC1 or an Immunosuppressive MSC2 Phenotype. PLoS ONE 5:e10088.
12. Rodrigues CE, JM Capcha, AC de Braganca, TR Sanches, PQ Gouveia, PA de Oliveira, DM Malheiros, RA Volpini, MA Santinho, BA Santana, RD Calado, IL Noronha and L Andrade. (2017). Human umbilical cord-derived mesenchymal stromal cells protect against premature renal senescence resulting from oxidative stress in rats with acute kidney injury. Stem Cell Res Ther 8:19.
13. Thomou T, MA Mori, JM Dreyfuss, M Konishi, M Sakaguchi, C Wolfrum, TN Rao, JN Winnay, R Garcia-Martin, SK Grinspoon, P Gorden and CR Kahn. (2017). Adipose-derived circulating miRNAs regulate gene expression in other tissues. Nature advance online publication.
14. Yu X, SL Harris and AJ Levine. (2006). The Regulation of Exosome Secretion: a Novel Function of the p53 Protein. Cancer Research 66:4795-4801.
15. Wiklander OP, JZ Nordin, A O'Loughlin, Y Gustafsson, G Corso, I Mager, P Vader, Y Lee, H Sork, Y Seow, N Heldring, L Alvarez-Erviti, CE Smith, K Le Blanc, P Macchiarini, P Jungebluth, MJ Wood and SE Andaloussi. (2015). Extracellular vesicle in vivo biodistribution is determined by cell source, route of administration and targeting. J Extracell Vesicles 4:26316.
16. Carraro G, L Perin, S Sedrakyan, S Giuliani, C Tiozzo, J Lee, G Turcatel, SP De Langhe, B Driscoll, S Bellusci, P Minoo, A Atala, RE De Filippo and D Warburton. (2008). Human amniotic fluid stem cells can integrate and differentiate into epithelial lung lineages. Stem Cells 26:2902-11.
17. Hauser PV, R De Fazio, S Bruno, S Sdei, C Grange, B Bussolati, C Benedetto and G Camussi. (2010). Stem cells derived from human amniotic fluid contribute to acute kidney injury recovery. Am J Pathol 177:2011-21.
18. Rota C, B Imberti, M Pozzobon, M Piccoli, P De Coppi, A Atala, E Gagliardini, C Xinaris, V Benedetti, AS Fabricio, E Squarcina, M Abbate, A Benigni, G Remuzzi and M Morigi. (2012). Human amniotic fluid stem cell preconditioning improves their regenerative potential. Stem Cells Dev 21:1911-23.
19. Bollini S, M Pozzobon, M Nobles, J Riegler, X Dong, M Piccoli, A Chiavegato, AN Price, M Ghionzoli, KK Cheung, A Cabrelle, PR O'Mahoney, E Cozzi, S Sartore, A Tinker, MF Lythgoe

Mary Ann Liebert Inc., 140 Huguenot Street, New Rochelle, NY 10801

and P De Coppi. (2011). In vitro and in vivo cardiomyogenic differentiation of amniotic fluid stem cells. Stem Cell Rev 7:364-80.

20. Pisciotta A, M Riccio, G Carnevale, A Lu, S De Biasi, L Gibellini, GB La Sala, G Bruzzesi, A Ferrari, J Huard and A De Pol. (2015). Stem cells isolated from human dental pulp and amniotic fluid improve skeletal muscle histopathology in mdx/SCID mice. Stem Cell Res Ther 6:156.
21. Piccoli M, C Franzin, E Bertin, L Urbani, B Blaauw, A Repele, E Taschin, A Cenedese, GF Zanon, I André-Schmutz, A Rosato, J Melki, M Cavazzana-Calvo, M Pozzobon and P De Coppi. (2012). Amniotic Fluid Stem Cells Restore the Muscle Cell Niche in a HSA-Cre, SmnF7/F7 Mouse Model. STEM CELLS 30:1675-1684.
22. De Coppi P, G Bartsch, MM Siddiqui, T Xu, CC Santos, L Perin, G Mostoslavsky, AC Serre, EY Snyder, JJ Yoo, ME Furth, S Soker and A Atala. (2007). Isolation of amniotic stem cell lines with potential for therapy. Nature Biotechnology 25:100-106.
23. Debacq-Chainiaux F, JD Erusalimsky, J Campisi and O Toussaint. (2009). Protocols to detect senescence-associated beta-galactosidase (SA-betagal) activity, a biomarker of senescent cells in culture and in vivo. Nat Protoc 4:1798-806.
24. Amthor H, A Otto, A Vulin, A Rochat, J Dumonceaux, L Garcia, E Mouisel, C Hourde, R Macharia, M Friedrichs, F Relaix, PS Zammit, A Matsakas, K Patel and T Partridge. (2009). Muscle hypertrophy driven by myostatin blockade does not require stem/precursor-cell activity. Proc Natl Acad Sci U S A 106:7479-84.
25. Diedrich B, KT Rigbolt, M Roring, R Herr, S Kaeser-Pebernard, C Gretzmeier, RF Murphy, T Brummer and J Dengjel. (2017). Discrete cytosolic macromolecular BRAF complexes exhibit distinct activities and composition. Embo j 36:646-663.
26. Cox J and M Mann. (2008). MaxQuant enables high peptide identification rates, individualized p.p.b.-range mass accuracies and proteome-wide protein quantification. Nat Biotechnol 26:1367-72.
27. Antonioli M, F Ciccosanti, J Dengjel and GM Fimia. (2017). Methods to Study the BECN1 Interactome in the Course of Autophagic Responses. Methods Enzymol 587:429-445.
28. Tyanova S, T Temu, P Sinitcyn, A Carlson, MY Hein, T Geiger, M Mann and J Cox. (2016). The Perseus computational platform for comprehensive analysis of (prote)omics data. Nat Methods 13:731-40.
29. Irizarry RA, B Hobbs, F Collin, YD Beazer-Barclay, KJ Antonellis, U Scherf and TP Speed. (2003). Exploration, normalization, and summaries of high density oligonucleotide array probe level data. Biostatistics 4:249-64.
30. Dweep H, C Sticht, P Pandey and N Gretz. (2011). miRWalk--database: prediction of possible miRNA binding sites by "walking" the genes of three genomes. J Biomed Inform 44:839-47.
31. Wang J, D Duncan, Z Shi and B Zhang. (2013). WEB-based GEne SeT AnaLysis Toolkit (WebGestalt): update 2013. Nucleic Acids Res 41:W77-83.
32. Simmonds RE and BM Foxwell. (2008). Signalling, inflammation and arthritis: NF-kappaB and its relevance to arthritis and inflammation. Rheumatology (Oxford) 47:584-90.
33. Eirin A, SM Riester, X-Y Zhu, H Tang, JM Evans, D O'Brien, AJ van Wijnen and LO Lerman. (2014). MicroRNA and mRNA cargo of extracellular vesicles from porcine adipose tissue-derived mesenchymal stem cells. Gene 551:55-64.
34. Camussi G, MC Deregibus, S Bruno, V Cantaluppi and L Biancone. (2010). Exosomes/microvesicles as a mechanism of cell-to-cell communication. Kidney Int 78:838-848.
35. Seok J-K, SH Lee, MJ Kim and Y-M Lee. (2014). MicroRNA-382 induced by HIF-1α is an angiogenic miR targeting the tumor suppressor phosphatase and tensin homolog. Nucleic Acids Research 42:8062-8072.
36. Yu G, Z Jia and Z Dou. (2017). miR-24-3p regulates bladder cancer cell proliferation, migration, invasion and autophagy by targeting DEDD. Oncol Rep 37:1123-1131.

Mary Ann Liebert Inc., 140 Huguenot Street, New Rochelle, NY 10801

37. Xia ZY, Y Hu, PL Xie, SY Tang, XH Luo, EY Liao, F Chen and H Xie. (2015). Runx2/miR-3960/miR-2861 Positive Feedback Loop Is Responsible for Osteogenic Transdifferentiation of Vascular Smooth Muscle Cells. Biomed Res Int 2015:624037.
38. Xu C, L Zhang, L Duan and C Lu. (2016). MicroRNA-3196 is inhibited by H2AX phosphorylation and attenuates lung cancer cell apoptosis by downregulating PUMA. Oncotarget 7:77764-77776.
39. Ma C, H Song, L Yu, K Guan, P Hu, Y Li, X Xia, J Li, S Jiang and F Li. (2016). miR-762 promotes porcine immature Sertoli cell growth via the ring finger protein 4 (RNF4) gene. Sci Rep 6:32783.
40. Yang D, Q Yuan, A Balakrishnan, H Bantel, J-H Klusmann, MP Manns, M Ott, T Cantz and AD Sharma. (2016). MicroRNA-125b-5p mimic inhibits acute liver failure. Nature Communications 7:11916.
41. Niu X, N Fu, J Du, R Wang, Y Wang, S Zhao, H Du, B Wang, Y Zhang, D Sun and Y Nan. (2016). miR-1273g-3p modulates activation and apoptosis of hepatic stellate cells by directly targeting PTEN in HCV-related liver fibrosis. FEBS Lett 590:2709-24.
42. Ti D, H Hao, C Tong, J Liu, L Dong, J Zheng, Y Zhao, H Liu, X Fu and W Han. (2015). LPS-preconditioned mesenchymal stromal cells modify macrophage polarization for resolution of chronic inflammation via exosome-shuttled let-7b. Journal of Translational Medicine 13:308.
43. Landskroner-Eiger S, I Moneke and WC Sessa. (2013). miRNAs as Modulators of Angiogenesis. Cold Spring Harbor Perspectives in Medicine 3:a006643.
44. Chang CP, CC Chio, CU Cheong, CM Chao, BC Cheng and MT Lin. (2013). Hypoxic preconditioning enhances the therapeutic potential of the secretome from cultured human mesenchymal stem cells in experimental traumatic brain injury. Clin Sci (Lond) 124:165-76.
45. Balbi C, M Piccoli, L Barile, A Papait, A Armirotti, E Principi, D Reverberi, L Pascucci, P Becherini, L Varesio, M Mogni, D Coviello, T Bandiera, M Pozzobon, R Cancedda and S Bollini. First Characterization of Human Amniotic Fluid Stem Cell Extracellular Vesicles as a Powerful Paracrine Tool Endowed with Regenerative Potential. STEM CELLS Translational Medicine:n/a-n/a.
46. Ferguson SW and J Nguyen. (2016). Exosomes as therapeutics: The implications of molecular composition and exosomal heterogeneity. J Control Release 228:179-190.
47. Collino F, MC Deregibus, S Bruno, L Sterpone, G Aghemo, L Viltono, C Tetta and G Camussi. (2010). Microvesicles derived from adult human bone marrow and tissue specific mesenchymal stem cells shuttle selected pattern of miRNAs. PloS One 5.
48. Deregibus MC, V Cantaluppi, R Calogero, M Lo Iacono, C Tetta, L Biancone, S Bruno, B Bussolati and G Camussi. (2007). Endothelial progenitor cell derived microvesicles activate an angiogenic program in endothelial cells by a horizontal transfer of mRNA. Blood 110:2440-2448.
49. Heijnen HF, AE Schiel, R Fijnheer, HJ Geuze and JJ Sixma. (1999). Activated platelets release two types of membrane vesicles: microvesicles by surface shedding and exosomes derived from exocytosis of multivesicular bodies and alpha-granules. Blood 94:3791-9.
50. Mathivanan S and RJ Simpson. (2009). ExoCarta: A compendium of exosomal proteins and RNA. Proteomics 9:4997-5000.
51. Lötvall J, AF Hill, F Hochberg, EI Buzás, D Di Vizio, C Gardiner, YS Gho, IV Kurochkin, S Mathivanan, P Quesenberry, S Sahoo, H Tahara, MH Wauben, KW Witwer and C Théry. (2014). Minimal experimental requirements for definition of extracellular vesicles and their functions: a position statement from the International Society for Extracellular Vesicles. Journal of Extracellular Vesicles 3:10.3402/jev.v3.26913.
52. Bangen JM, FU Schade and SB Flohé. (2007). Diverse regulatory activity of human heat shock proteins 60 and 70 on endotoxin-induced inflammation. Biochemical and Biophysical Research Communications 359:709-715.

Mary Ann Liebert Inc., 140 Huguenot Street, New Rochelle, NY 10801

53. Danzer KM, WP Ruf, P Putcha, D Joyner, T Hashimoto, C Glabe, BT Hyman and PJ McLean. (2011). Heat-shock protein 70 modulates toxic extracellular α-synuclein oligomers and rescues trans-synaptic toxicity. The FASEB Journal 25:326-336.
54. Bianchi ME. (2007). DAMPs, PAMPs and alarmins: all we need to know about danger. J Leukoc Biol 81:1-5.
55. Chen Y, G Li, Y Liu, VP Werth, KJ Williams and M-L Liu. (2016). Translocation of Endogenous Danger Signal HMGB1 From Nucleus to Membrane Microvesicles in Macrophages. Journal of Cellular Physiology 231:2319-2326.
56. Perdiguero E, P Sousa-Victor, V Ruiz-Bonilla, M Jardí, C Caelles, AL Serrano and P Muñoz-Cánoves. (2011). p38/MKP-1–regulated AKT coordinates macrophage transitions and resolution of inflammation during tissue repair. The Journal of Cell Biology 195:307-322.
57. Lee Y, SR Sooranna, V Terzidou, M Christian, J Brosens, K Huhtinen, M Poutanen, G Barton, MR Johnson and PR Bennett. (2012). Interactions between inflammatory signals and the progesterone receptor in regulating gene expression in pregnant human uterine myocytes. Journal of Cellular and Molecular Medicine 16:2487-2503.
58. Lim S, DA MacIntyre, YS Lee, S Khanjani, V Terzidou, TG Teoh and PR Bennett. (2012). Nuclear factor kappa B activation occurs in the amnion prior to labour onset and modulates the expression of numerous labour associated genes. PLoS One 7:e34707.
59. Kim SH, DA MacIntyre, M Firmino Da Silva, AM Blanks, YS Lee, S Thornton, PR Bennett and V Terzidou. (2015). Oxytocin activates NF-kappaB-mediated inflammatory pathways in human gestational tissues. Mol Cell Endocrinol 403:64-77.
60. Morelli AE, AT Larregina, WJ Shufesky, ML Sullivan, DB Stolz, GD Papworth, AF Zahorchak, AJ Logar, Z Wang, SC Watkins, LD Falo, Jr. and AW Thomson. (2004). Endocytosis, intracellular sorting, and processing of exosomes by dendritic cells. Blood 104:3257-66.
61. Ronquist KG, C Sanchez, L Dubois, D Chioureas, P Fonseca, A Larsson, A Ullén, J Yachnin, G Ronquist and T Panaretakis. (2016). Energy-requiring uptake of prostasomes and PC3 cell-derived exosomes into non-malignant and malignant cells. Journal of Extracellular Vesicles 5:10.3402/jev.v5.29877.
62. Villarroya-Beltri C, C Gutierrez-Vazquez, F Sanchez-Cabo, D Perez-Hernandez, J Vazquez, N Martin-Cofreces, DJ Martinez-Herrera, A Pascual-Montano, M Mittelbrunn and F Sanchez-Madrid. (2013). Sumoylated hnRNPA2B1 controls the sorting of miRNAs into exosomes through binding to specific motifs. Nat Commun 4:2980.
63. Alvarez ML, M Khosroheidari, R Kanchi Ravi and JK DiStefano. (2012). Comparison of protein, microRNA, and mRNA yields using different methods of urinary exosome isolation for the discovery of kidney disease biomarkers. Kidney Int 82:1024-1032.
64. Valadi H, K Ekström, A Bossios, M Sjöstrand, JJ Lee and JO Lötvall. (2007). Exosome-mediated transfer of mRNAs and microRNAs is a novel mechanism of genetic exchange between cells. Nature Cell Biology 9:654-659.
65. Lo Sicco C, D Reverberi, C Balbi, V Ulivi, E Principi, L Pascucci, P Becherini, MC Bosco, L Varesio, C Franzin, M Pozzobon, R Cancedda and R Tasso. (2017). Mesenchymal Stem Cell-Derived Extracellular Vesicles as Mediators of Anti-Inflammatory Effects: Endorsement of Macrophage Polarization. STEM CELLS Translational Medicine:n/a-n/a.
66. Lu H, X Lei and Q Zhang. (2015). Moderate activation of IKK2-NF-kB in unstressed adult mouse liver induces cytoprotective genes and lipogenesis without apparent signs of inflammation or fibrosis. BMC Gastroenterology 15:94.
67. Zhang Y, J Liu, S Yao, F Li, L Xin, M Lai, V Bracchi-Ricard, H Xu, W Yen, W Meng, S Liu, L Yang, S Karmally, J Liu, H Zhu, J Gordon, K Khalili, S Srinivasan, JR Bethea, X Mo and W Hu. (2012). Nuclear Factor Kappa B Signaling Initiates Early Differentiation of Neural Stem Cells. STEM CELLS 30:510-524.
68. Omairi S, A Matsakas, H Degens, O Kretz, K-A Hansson, AV Solbrå, JC Bruusgaard, B Joch, R Sartori, N Giallourou, R Mitchell, H Collins-Hooper, K Foster, A Pasternack, O Ritvos, M

Sandri, V Narkar, JR Swann, TB Huber and K Patel. (2016). Enhanced exercise and regenerative capacity in a mouse model that violates size constraints of oxidative muscle fibres. eLife 5:e16940.

69. Zammit PS, JP Golding, Y Nagata, V Hudon, TA Partridge and JR Beauchamp. (2004). Muscle satellite cells adopt divergent fates: a mechanism for self-renewal? J Cell Biol 166:347-57.

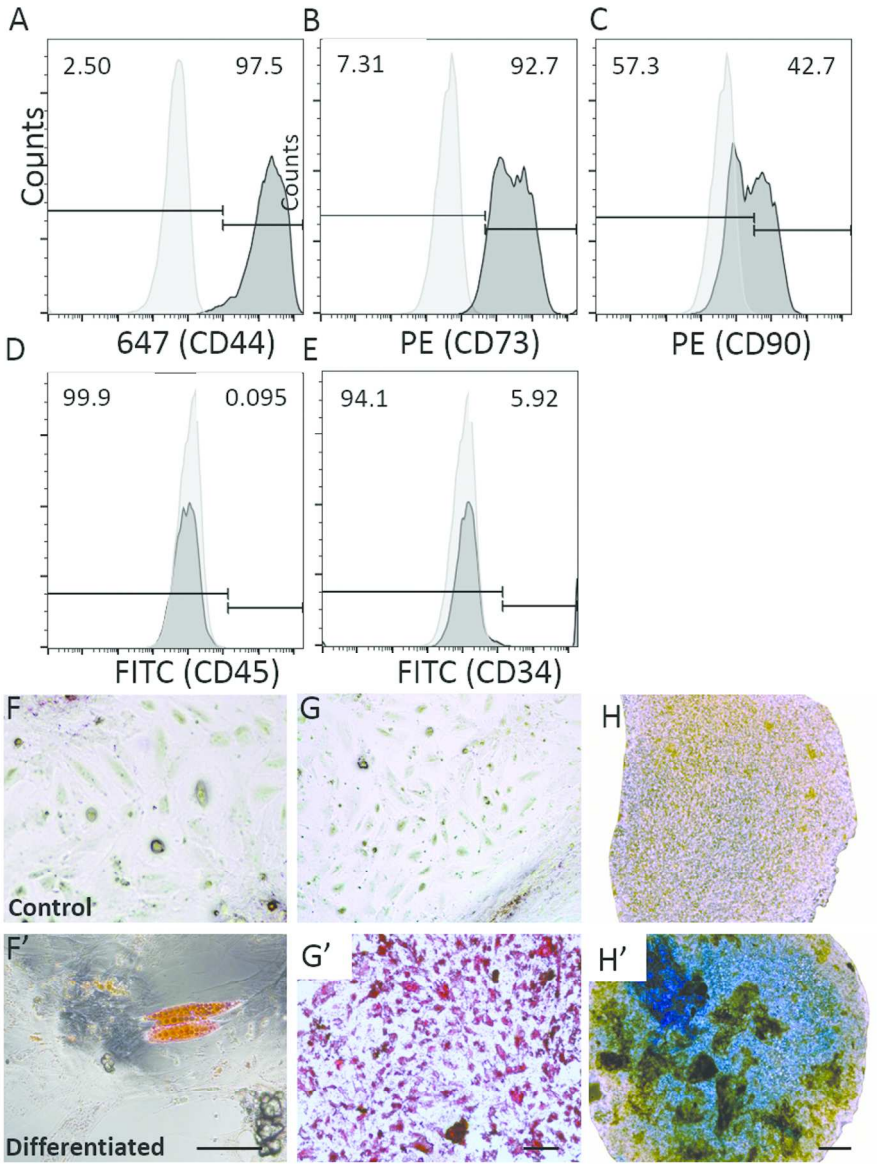

Figure 1: AF-CM content and multipotency of post-CM generated AFSCs. Flow cytometry analysis for (A) CD44 (B) CD73, (C) CD90 (D) CD45, (E) CD34. (F-H) AFSCs cultured in growth media. AFSCs cultured in adipogenic (F') osteogenic (G') and chondrogenic (H') media. (F, H) Scale bar equal to 50μm, (H) equals 100μm.

150x198mm (300 x 300 DPI)

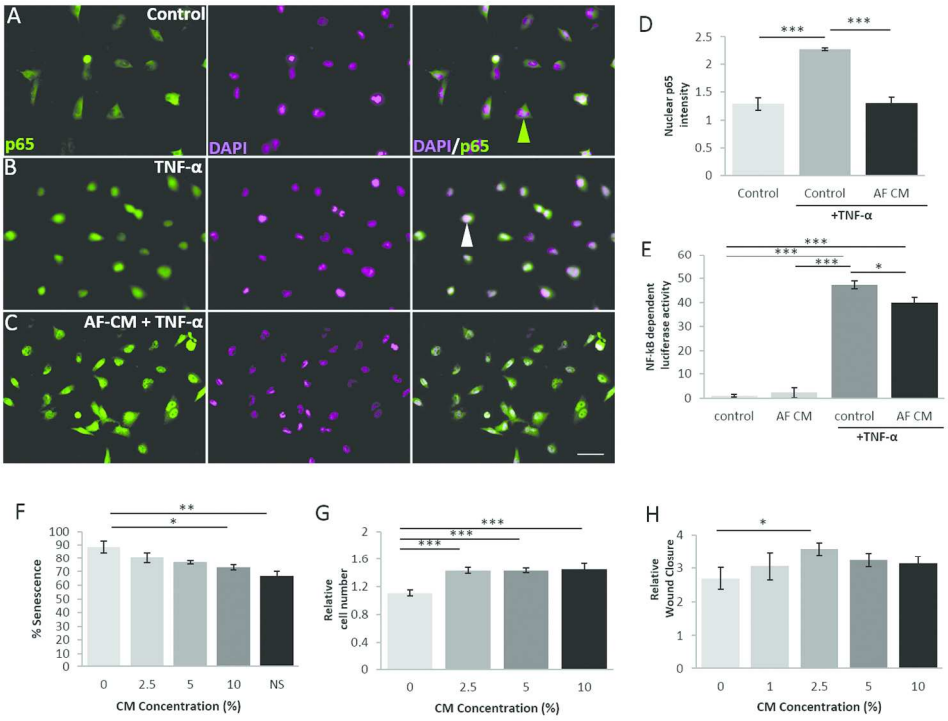

Figure 2: In-vitro assessment of biological activity of whole AF-CM. (A-C) U251 cells stained for NF-κB-p65 (green) (n=4). (D) Nuclear translocation of p65 analysed by intensity measurement. Green and white arrows representative of weak and strong nuclear localisation respectively. (E) NF-κB quantification. (F) Protection against H2O2-induced senescence compared to non-stressed U251 cells (NS). (G) Cell number relative to controls (0%). (H) Wound closure assay. (A-C) Images taken at 20x Magnification. Scale represents 50µm. Values are expressed as mean ± SEM (n=4). $p < 0.05$ (*), $p < 0.01$ (**) or $p < 0.001$ (***)

199x160mm (300 x 300 DPI)

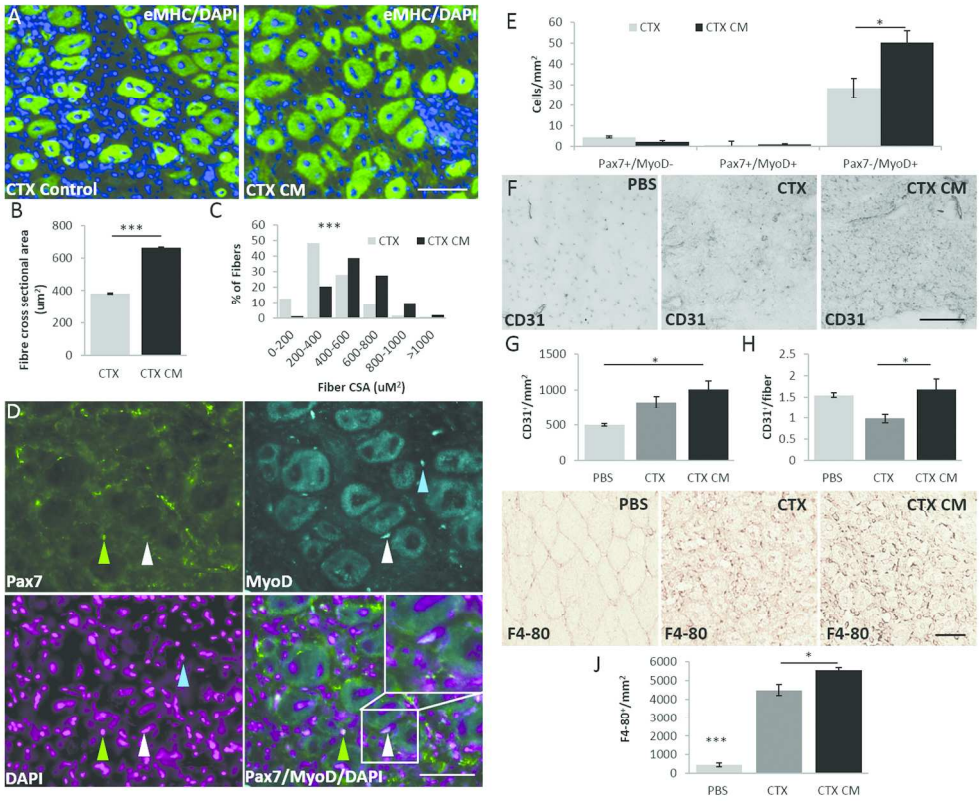

Figure 3: AF-CM and muscle regeneration. (A) embryonic Myosin heavy chain expression in damaged muscle (green). (B) Quantification of cross sectional area of newly regenerated fibres. (C) Frequency distribution graph of regenerated muscle fibres. (D) Immunofluorescent staining for Pax7 (green), MyoD (Cyan) and DAPI (Magenta). (E) Quantification of quiescent satellite Pax-7+/MyoD-, activated satellite cells Pax-7+/MyoD+ and muscle lineage committed progenitor cells Pax-7-/MyoD+. (F) CD31 staining for capillaries in regenerating muscle. (G) Quantification of capillary density (number per mm2) and (H) quantification per fibre. (I) F4-80 staining for macrophages (J) damaged areas assessed for the number of F4-80+ cells. Black arrows indicate F4-80+ cells. (A) Scale bars are equal to 100μm. (D, F, I) Scale bar represents 50μm. Values are expressed as means ± SEM (n=5). $p < 0.05$ (*), $p < 0.01$ (**) or $p < 0.001$ (***)

199x164mm (300 x 300 DPI)

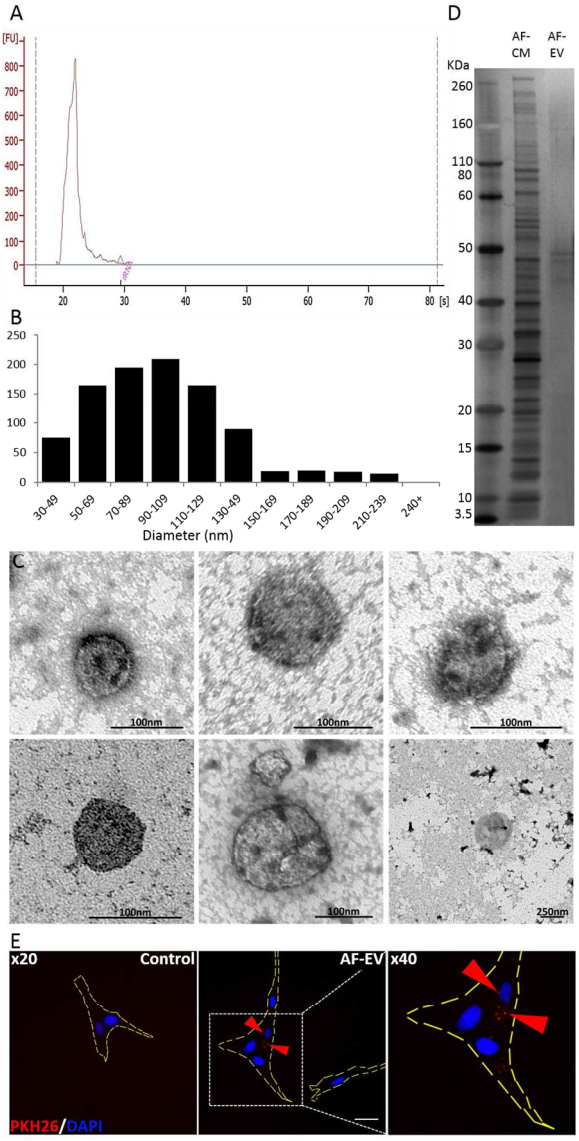

Figure 4: Characterisation of AF-CM and AF-EV fraction. (A) Bioanalyser profile of RNA size (s) and frequency (FU) in AF-EV. (B) Size-frequency distribution plot of AF-EVs. (C) Electron micrograph images of AF-EV. (D) AF-CM and AF-EV fraction protein silver staining. (E) Uptake of PKH26+ AF-EV (red) by IMR-90 cells (red arrows). (E) Scale bar representative of 20μm. $p < 0.05$ (*), $p < 0.01$ (**) or $p < 0.001$ (***)

150x265mm (300 x 300 DPI)

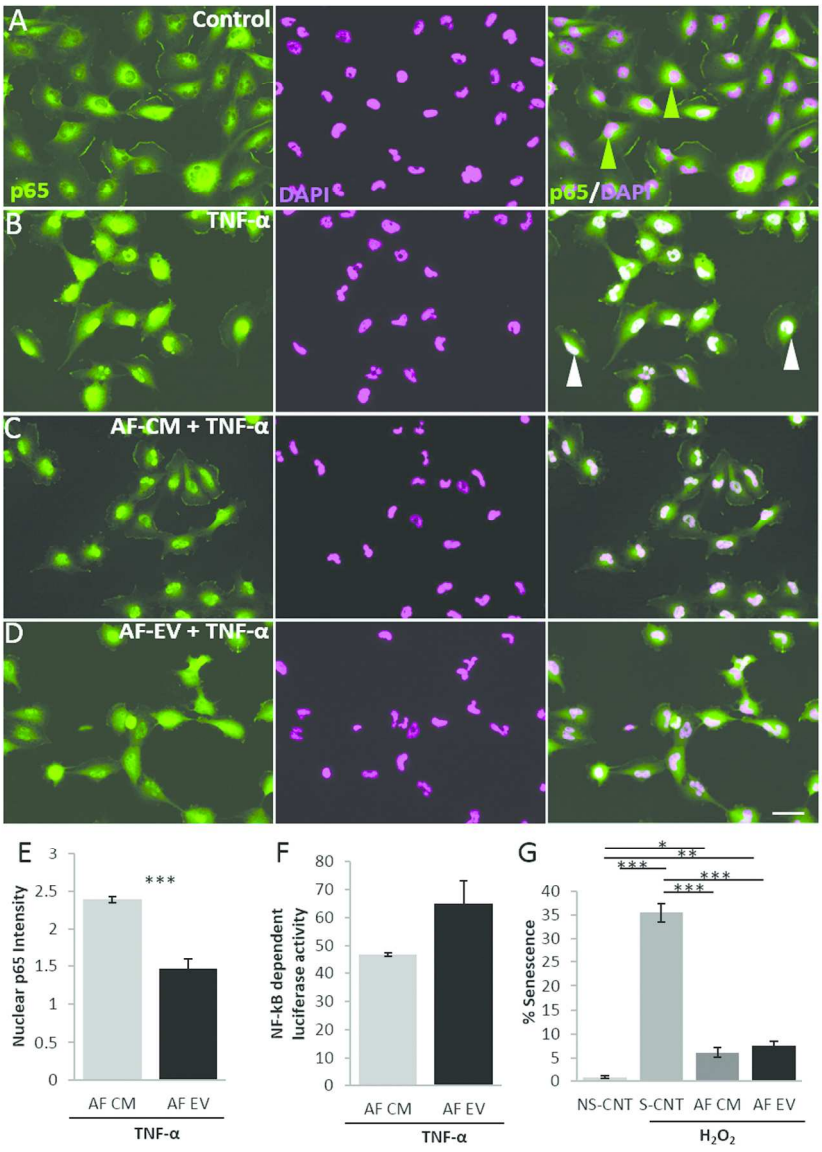

Figure 5: In-vitro assessment of biological activity of AF-EV. (A-D) U251 cells stained for NF-κB-p65 (green) immunofluorescence (n=4). (E) Nuclear translocation of p65 analysed by intensity measurement. (F) NF-κB quantification. (G) H2O2 Stressed IMR-90 cells treated with AF-CM or AF-EV CM compared to a non-stressed control (NS). Images were taken at a 20x Magnification. Green and white arrows representative of weak and strong nuclear localisation respectively. Scale bar represent 50μm. Values are expressed as means ± SEM (n=4). $p < 0.05$ (*), $p < 0.01$ (**) or $p < 0.001$ (***)

150x192mm (300 x 300 DPI)

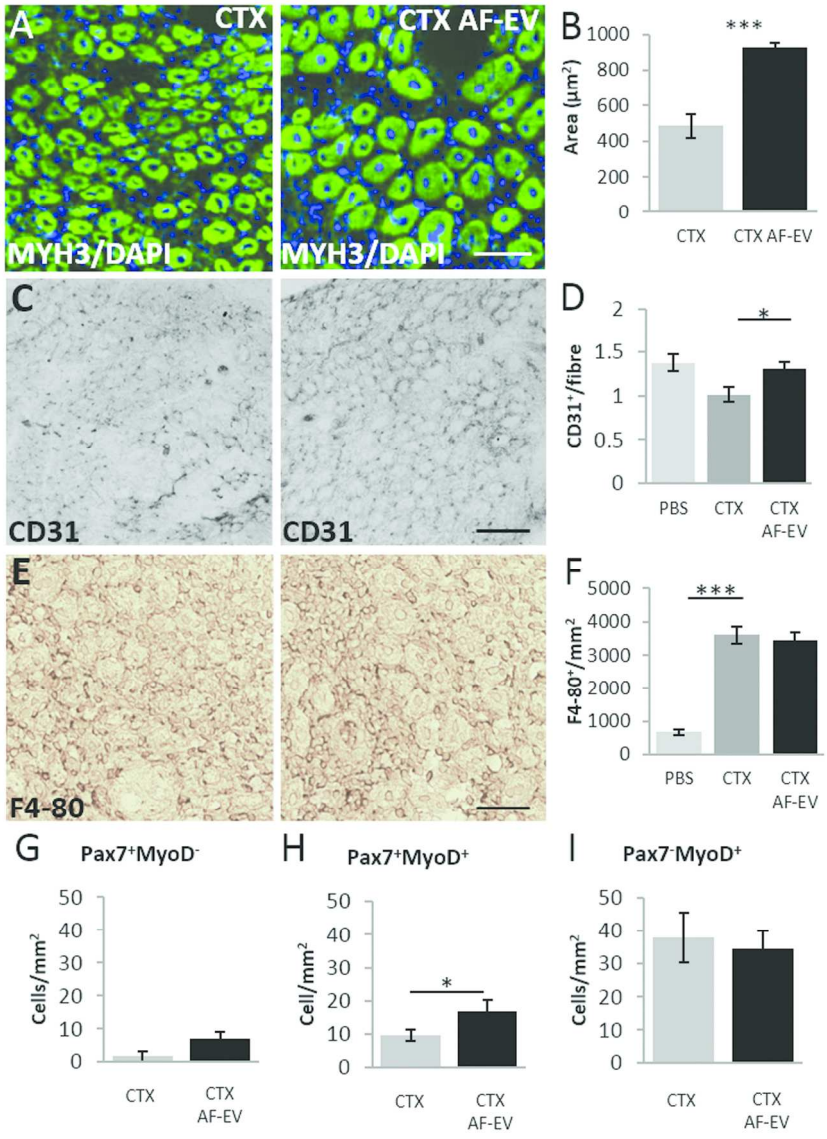

Figure 6: AF-EV and muscle regeneration. (A) embryonic Myosin heavy chain expression in damaged muscle (green). (B) Quantification of cross sectional area of newly regenerated fibres. (C) CD31 staining for capillaries in regenerating muscle. (D) Quantification of CD31+ capillaries per fibre. (E) F4-80 staining for macrophages. (F) Damaged areas assessed for the number of positive F4-80 cells/mm2. Comparison of the number of Pax-7+/MyoD- quiescent satellite cells (G), Pax-7+/MyoD+ activated satellite cells (H) and Pax-7-/MyoD+ muscle lineage committed progenitor cells (I) per mm2 between treated groups. Values are expressed as means ± SEM (n=5). (A) Scale bar equal to 100µm. (C, E) Scale bar represent 50µm. $p < 0.05$ (*), $p < 0.01$ (**) or $p < 0.001$ (***)

150x206mm (300 x 300 DPI)

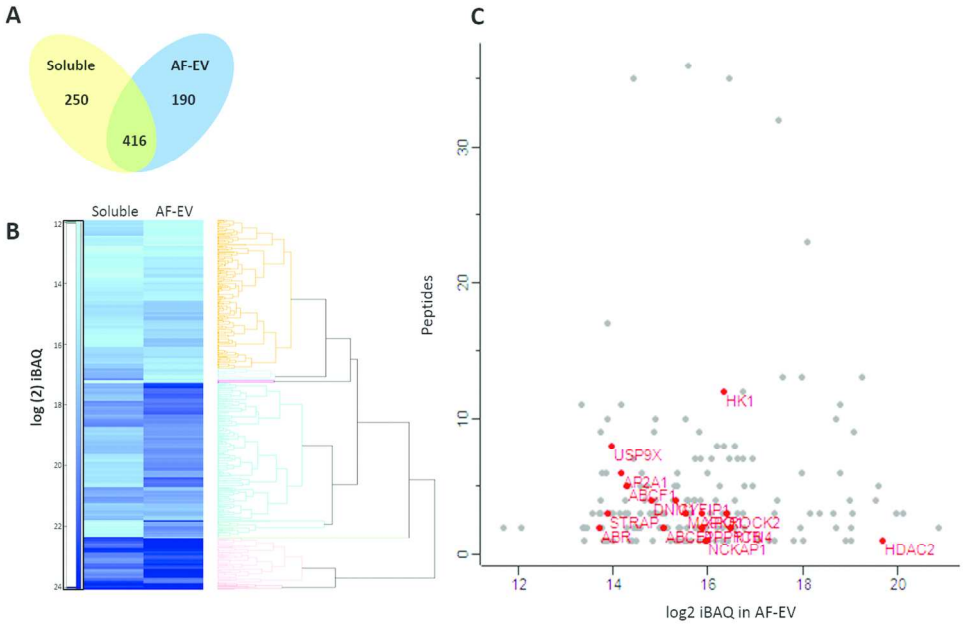

Figure 7: Mass spectrometry analysis and comparison between the AF-EV and AF CM soluble fraction. (A) Number of proteins shared and specific to the AF-EV or soluble fraction. (B) Heat map of GO-terms found in the AF-EV and resulting soluble fraction. (C) Transmembrane transporters and receptors enriched in AF-EV fraction.

150x100mm (300 x 300 DPI)

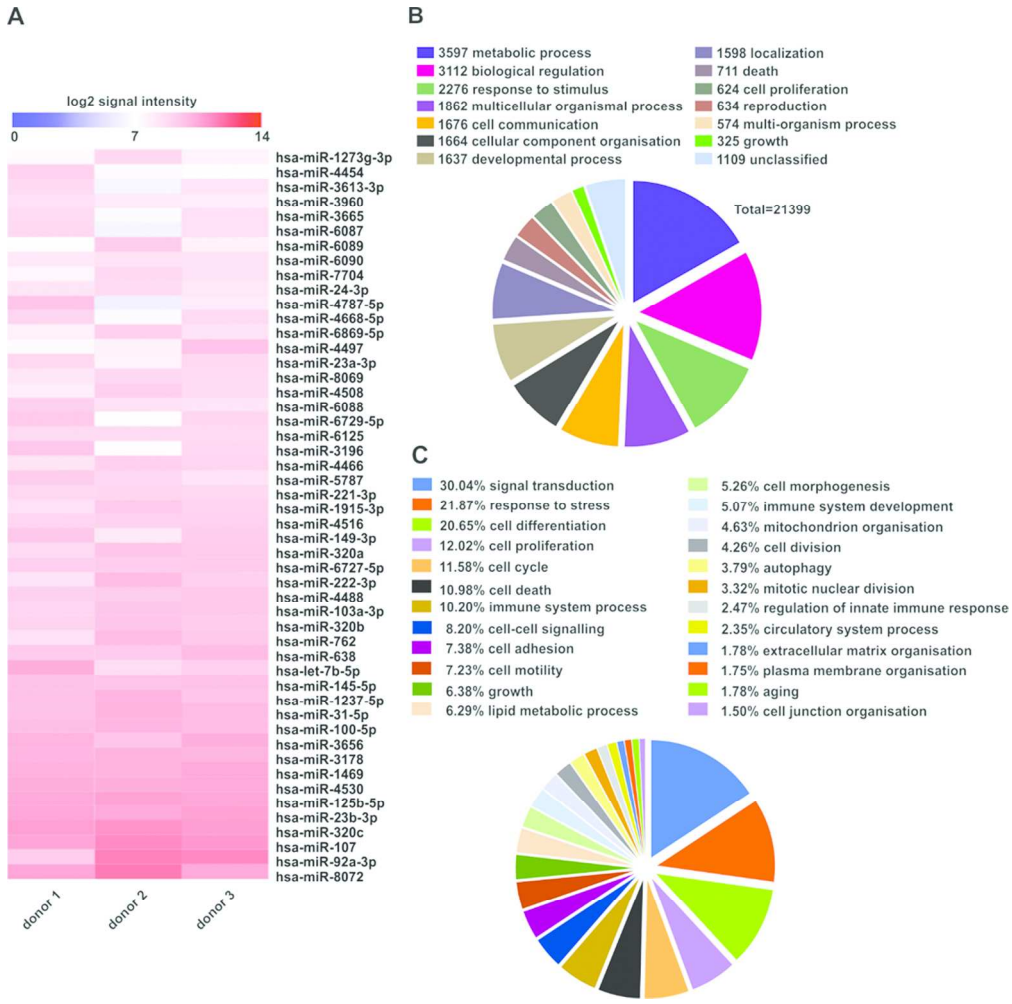

Figure 8: Profiling of AF-EV miRNA content (n=3). (A) Top 50 expressed miRNAs. (B) General cell processes targeted by all miRNA present. (C) Specific cellular processes and signalling pathways targeted by the miRNA present.

150x148mm (300 x 300 DPI)

Legends

Figure 1: AF-CM content and multipotency of post-CM generated AFSCs. Flow cytometry analysis for **(A)** CD44 **(B)** CD73, **(C)** CD90 **(D)** CD45, **(E)** CD34. **(F-H)** AFSCs cultured in growth media. AFSCs cultured in adipogenic **(F')** osteogenic **(G')** and chondrogenic **(H')** media**. (F, H)** Scale bar equal to 50µm, **(H)** equals 100µm.

Figure 2: In-vitro assessment of biological activity of whole AF-CM. **(A-C)** U251 cells stained for NF-κB-p65 (green) (n=4). **(D)** Nuclear translocation of p65 analysed by intensity measurement. Green and white arrows representative of weak and strong nuclear localisation respectively. **(E)** NF-κB quantification. **(F)** Protection against H_2O_2-induced senescence compared to non-stressed U251 cells (NS). **(G)** Cell number relative to controls (0%). **(H)** Wound closure assay. (A-C) Images taken at 20x Magnification. Scale represents 50µm. Values are expressed as mean ± SEM (n=4). $p < 0.05$ (*), $p < 0.01$ (**) or $p < 0.001$ (***)

Figure 3: AF-CM and muscle regeneration. (**A**) embryonic Myosin heavy chain expression in damaged muscle (green). (**B**) Quantification of cross sectional area of newly regenerated fibres. (**C**) Frequency distribution graph of regenerated muscle fibres. (**D**) Immunofluorescent staining for Pax7 (green), MyoD (Cyan) and DAPI (Magenta). (**E**) Quantification of quiescent satellite Pax-7^+/MyoD$^-$, activated satellite cells Pax-7^+/MyoD$^+$ and muscle lineage committed progenitor cells Pax-7^-/MyoD$^+$. (**F**) CD31 staining for capillaries in regenerating muscle. (**G**) Quantification of capillary density (number per mm^2) and **(H)** quantification per fibre. (**I**) F4-80 staining for macrophages (**J**) damaged areas assessed for the number of F4-80^+ cells. Black arrows indicate F4-80^+ cells. **(A)** Scale bars are equal to 100µm. **(D, F, I)** Scale bar represents 50µm. Values are expressed as means ± SEM (n=5). $p < 0.05$ (*), $p < 0.01$ (**) or $p < 0.001$ (***)

Figure 4: Characterisation of AF-CM and AF-EV fraction. **(A)** Bioanalyser profile of RNA size (s) and frequency (FU) in AF-EV. **(B)** Size-frequency distribution plot of AF-EVs. **(C)** Electron micrograph images of AF-EV. **(D)** AF-CM and AF-EV fraction protein silver staining. **(E)** Uptake of PKH26^+ AF-EV (red) by IMR-90 cells (red arrows). **(E)** Scale bar representative of 20µm. $p < 0.05$ (*), $p < 0.01$ (**) or $p < 0.001$ (***)

Figure 5: In-vitro assessment of biological activity of AF-EV. **(A-D)** U251 cells stained for NF-κB-p65 (green) immunofluorescence (n=4). **(E)** Nuclear translocation of p65 analysed by intensity measurement. **(F)** NF-κB quantification. **(G)** H_2O_2 Stressed IMR-90 cells treated with AF-CM or AF-EV CM compared to a non-stressed control (NS). Images were taken at a 20x Magnification. Green and white arrows representative of weak and strong nuclear localisation respectively. Scale bar

represent 50µm. Values are expressed as means ± SEM (n=4). $p < 0.05$ (*), $p < 0.01$ (**) or $p < 0.001$ (***)

Figure 6: AF-EV and muscle regeneration. (**A**) embryonic Myosin heavy chain expression in damaged muscle (green). (**B**) Quantification of cross sectional area of newly regenerated fibres. **(C)** CD31 staining for capillaries in regenerating muscle. **(D)** Quantification of $CD31^+$ capillaries per fibre. **(E)** F4-80 staining for macrophages. **(F)** Damaged areas assessed for the number of positive F4-80 cells/mm^2. Comparison of the number of $Pax\text{-}7^+/MyoD^-$ quiescent satellite cells **(G),** $Pax\text{-}7^+/MyoD^+$ activated satellite cells **(H)** and $Pax\text{-}7^-/MyoD^+$ muscle lineage committed progenitor cells **(I)** per mm^2 between treated groups. Values are expressed as means ± SEM (n=5). **(A)** Scale bar equal to 100µm. **(C, E)** Scale bar represent 50µm. $p < 0.05$ (*), $p < 0.01$ (**) or $p < 0.001$ (***)

Figure 7: Mass spectrometry analysis and comparison between the AF-EV and AF CM soluble fraction. **(A)** Number of proteins shared and specific to the AF-EV or soluble fraction. **(B)** Heat map of GO-terms found in the AF-EV and resulting soluble fraction. **(C)** Transmembrane transporters and receptors enriched in AF-EV fraction.

Figure 8: Profiling of AF-EV miRNA content (n=3). **(A)** Top 50 expressed miRNAs. **(B)** General cell processes targeted by all miRNA present. **(C)** Specific cellular processes and signalling pathways targeted by the miRNA present.

Supplementary Figure 1: **(A)** Flow cytometry analysis of AFSCs post CM collection for original selection marker CD117. **(B)** IMR-90 cells stained for senescence associated beta-galactosidase following H_2O_2 induced stress. Scale bar equal to 20µm

Table. 1 Soluble and Extracellular Vesicles GOMF terms enrichment

Category value	Selection size	Category size	Enrichment factor	P value	Benj. Hoch. FDR
nucleic acid metabolic process	112	126	2,5057	2,66E-33	8,10E-27
RNA metabolic process	112	105	2,6531	2,88E-30	4,38E-24
metabolic process	192	297	1,3423	9,33E-28	9,46E-22
proteolysis	32	42	8,3571	8,10E-27	4,92E-21
Aminoacyl-tRNA biosynthesis	13	13	32	6,73E-25	8,87E-20
proteolysis	21	42	9,9048	4,58E-24	9,29E-19
small molecule metabolic process	192	112	1,8571	5,27E-24	1,00E-18
tRNA metabolic process	13	14	29,714	9,43E-24	1,51E-18
nucleobase-containing compound metabolic process	112	159	2,0323	1,03E-23	1,56E-18
ribonucleoprotein complex	78	58	3,8621	3,95E-23	1,74E-17
regulation of gene expression	112	107	2,3605	1,74E-21	2,52E-16
cytoskeleton	49	81	3,9829	1,24E-21	2,73E-16
nucleic acid metabolic process	48	126	3,0265	2,17E-21	3,00E-16
ncRNA metabolic process	13	18	23,111	5,77E-21	7,02E-16
primary metabolic process	192	279	1,3357	6,13E-21	7,17E-16
regulation of RNA metabolic process	112	78	2,619	1,05E-19	1,18E-14
RNA processing	78	42	4,1905	1,85E-19	2,01E-14
regulation of catalytic activity	29	62	5,7842	2,53E-19	2,66E-14
nitrogen compound metabolic process	112	183	1,8064	3,14E-19	3,19E-14
cellular nitrogen compound metabolic process	112	180	1,8159	4,90E-19	4,81E-14
regulation of RNA metabolic process	48	78	3,8889	6,94E-19	6,59E-14
mRNA metabolic process	78	46	3,942	1,33E-18	1,23E-13
RNA processing	112	42	3,2721	1,44E-18	1,29E-13
mRNA metabolic process	112	46	3,1491	2,33E-18	2,02E-13

Mary Ann Liebert Inc., 140 Huguenot Street, New Rochelle, NY 10801

Table. 2 Soluble only GOMF terms enrichment

Category value	Selection	Category	Enrichment factor	P value	Benj. Hoch. FDR
translational initiation	13	12	17,628	1,94E-16	3,05E-10
regulation of translational initiation	13	10	19,231	1,31E-15	1,02E-09
translational initiation	15	12	15,278	3,37E-15	1,76E-09
regulation of gene expression	46	63	2,9331	4,56E-15	1,79E-09
regulation of translational initiation	15	10	16,667	1,37E-14	3,07E-09
regulation of macromolecule biosynthetic process	46	53	3,1788	1,21E-14	3,16E-09
regulation of cellular macromolecule biosynthetic process	46	53	3,1788	1,21E-14	3,79E-09
regulation of cellular biosynthetic process	46	55	3,0632	5,54E-14	9,66E-09
regulation of biosynthetic process	46	55	3,0632	5,54E-14	1,09E-08
nucleic acid metabolic process	23	47	4,6253	6,93E-14	1,09E-08
translational initiation	26	12	9,6154	1,01E-13	1,33E-08
regulation of translation	15	14	13,095	9,88E-14	1,41E-08
regulation of transcription, DNA-dependent	23	38	5,1487	5,90E-13	7,12E-08
translation	13	10	17,308	7,74E-13	8,67E-08
regulation of translation	13	14	13,736	1,24E-12	1,30E-07

Mary Ann Liebert Inc., 140 Huguenot Street, New Rochelle, NY 10801

Table. 3 Extracellular Vesicles only GOMF terms enrichment

Category value	Selection	Category	Enrichment factor	P value	Benj. Hoch. FDR
Ribosome	28	28	6,7857	3,87E-34	2,17E-29
viral transcription	28	28	6,7857	3,87E-34	8,96E-29
translational termination	28	28	6,7857	3,87E-34	1,20E-28
protein complex disassembly	28	28	6,7857	3,87E-34	1,79E-28
cellular protein complex disassembly	28	28	6,7857	3,87E-34	3,58E-28
viral reproductive process	28	29	6,5517	1,12E-32	1,16E-27
viral infectious cycle	28	29	6,5517	1,12E-32	1,30E-27
translational elongation	28	29	6,5517	1,12E-32	1,49E-27
macromolecular complex disassembly	28	29	6,5517	1,12E-32	1,73E-27
cellular macromolecular complex disassembly	28	29	6,5517	1,12E-32	2,08E-27
SRP-dependent cotranslational protein targeting to membrane	28	30	6,3333	1,68E-31	1,04E-26
protein targeting to membrane	28	30	6,3333	1,68E-31	1,11E-26
protein targeting to ER	28	30	6,3333	1,68E-31	1,20E-26
nuclear-transcribed mRNA catabolic process	28	30	6,3333	1,68E-31	1,30E-26
establishment of protein localization in endoplasmic reticulum	28	30	6,3333	1,68E-31	1,42E-26

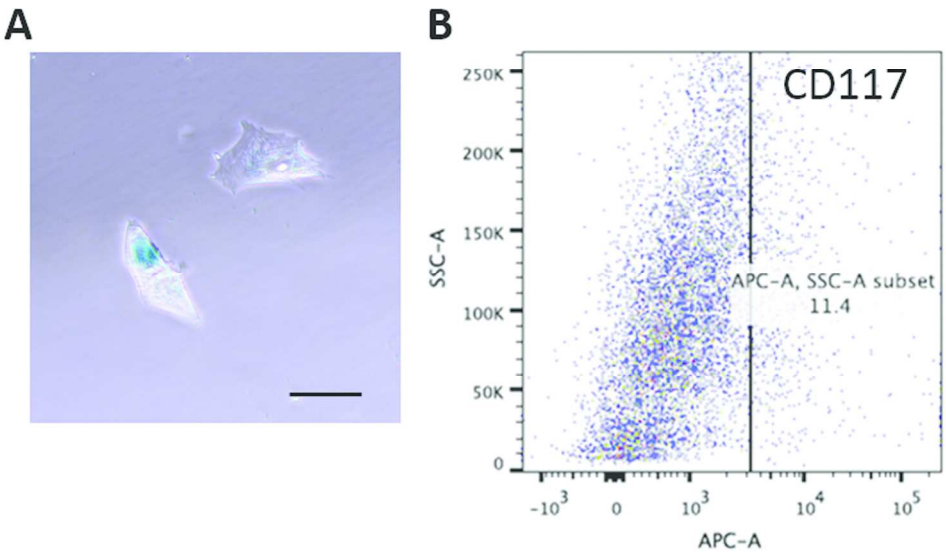

Supplementary Figure 1: (A) Flow cytometry analysis of AFSCs post CM collection for original selection marker CD117. (B) IMR-90 cells stained for senescence associated beta-galactosidase following H2O2 induced stress. Scale bar equal to 20μm

150x91mm (300 x 300 DPI)